

Anhalt University of Applied Sciences
Institute for Membrane and Shell Technologies, Building and Real Estate

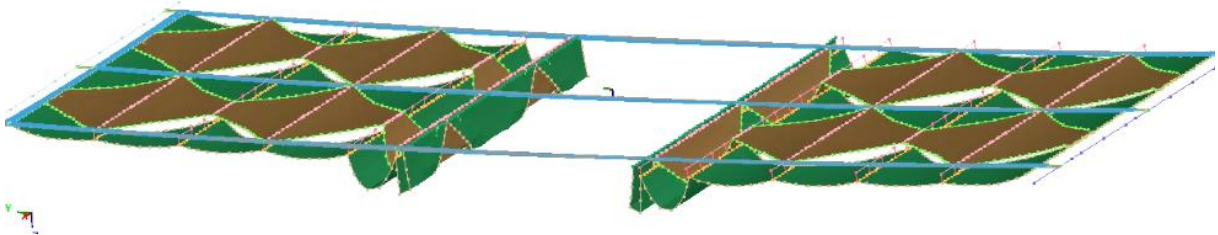
Master in Membrane and Shell Structures

On the Dynamic behavior of the Pre-Stressed Flat Membrane Structures

Raham Zarfam

Prof. Dr.-Ing. K.-U. Bletzinger, Prof. Dr.-Ing. R. Off

March 2017



Abstract

A pre-stressed cable-supported flat membrane structure is considered under wind load. The structure is studied parametrically under different cable pretensions to uncover various ranges of structural properties. Computational Fluid Dynamic (CFD) approach is applied to evaluate the pressure distribution on the membrane skin and Computational Structural Dynamic (CSD) is used to compute the dynamic responses of the structure. Several numerical approaches based on CFD and CSD methods are utilized to simulate the structure considering the material nonlinearity and large deformation behavior of the structural members. Furthermore, Fluid Structure Interaction (FSI) simulation is applied in this study and its results are considered as the reference to evaluate other numerical methods. A simplified numerical method is proposed by calibrating the structural properties of CSD model in order to consider the effect of the air added mass and aerodynamic damping. The results show the efficiency of the proposed method in increasing the precision of the structural response by avoiding the costly FSI simulation.

Acknowledgements

Special Thanks to Dr.-Ing Alexander Michalski, Ramakrishna Nanjundaiah and Atis Degro from SL Rasch GmbH and also Dr. Eberhard Haug from ESI group for their technical supports in forming this research study.

I would like to gratefully thank my advisor professor, Dr.-Ing Kai-Uwe Bletzinger and Dr.-Ing Robert Off for their valuable knowledge and experience in the field of numerical simulation and membrane structures from which I learnt at Institute of Membrane and Shell Structures in Anhalt University of Applied Science.

It is a pleasure to acknowledge Mustafa Rasch and Jürgen Bradatsch, the CEO and CTO of SL Rasch GmbH for giving me this unique opportunity to work on this research topic. Only with their cooperation this work is made possible.

Biography

Raham Zarfam is R&D structural engineer at SL Rasch GmbH with 4 years of profound experience in development, analysis, design of lightweight structures from high span retractable membrane Skins to glass-fiber roof shell. Furthermore, he has six years practical experience in analysis, design, seismic evaluation and retrofitting of steel and concrete structures. He has received his PhD degree in structural and earthquake engineering in 2011 from Sharif University of Technology, Iran. He has performed research in the areas of structural control and dynamics in addition to computational wind engineering of wide span tensile structures.

Table of Contents

- 1 Introduction 4
 - 1.1 History and background 4
 - 1.2 Stiffness of the tensile membrane structures 7
 - 1.3 Dynamic simulation of prestressed membrane structures in the Literature..... 8
- 2 Flat pre-stressed membrane structure 10

In the following table, the information about the weight of each structural member is presented.
The weight of the edge belt is negligible. 11

 - 2.1 The effect of pre-tension..... 11
 - 2.2 Eigen-frequency 13
 - 2.2.1 Frequency - Pretension 17
- 3 The Aero-dynamic effect on the dynamic characteristic of toldo..... 18
 - 3.1 Free Oscillation..... 18
 - 3.1.1 Definition of the added mass and aerodynamic damping 20
 - 3.2 Calibration of CSD model corresponding to FSI 21
- 4 Wind simulation 22
 - 4.1 Design wind speed for convertible toldo structures 22
 - 4.2 CSD simulation..... 22
 - 4.2.1 CFD simulation..... 23
 - 4.2.2 CSD simulation..... 25
 - 4.3 FSI simulation 29
 - 4.3.1 CFD mesh..... 30
 - 4.4 Simulation of the calibrated CSD model 36
- 5 Evaluation of the results and conclusion 38
 - 5.1 Static analysis according to Eurocode 38
 - 5.2 Quasi-static analysis under extreme value of the wind pressure governed from CFD-only simulation..... 40
 - 5.3 Results comparison and evaluation 41
- References..... 43

1 Introduction

In this chapter, the application of the retractable roofs from past till now is briefly described and the important research studies in this area are introduced.

One type of retractable membrane roof is toldo structures which are shown in the following figure [3]. Generally, this structural system consists of foldable membrane and supporting cables. The moving mechanism is provided by some sliding elements which are connecting the membrane to the supporting cables. The additional cable system is needed to drive one membrane edge forward and backward in order to fold or deploy the roof. The curvature of membrane in this type of roof normally is not high. Therefore, the membrane skin is almost flat and this leads to high membrane deformation normal to the skin face under loading perpendicular to the membrane. In order to limit the membrane against such movement, the higher pretension is applied on membrane or on supporting cables. However, despite of prestressing the structural system the movement of the membrane can be problematic and serious in case of wind loads.

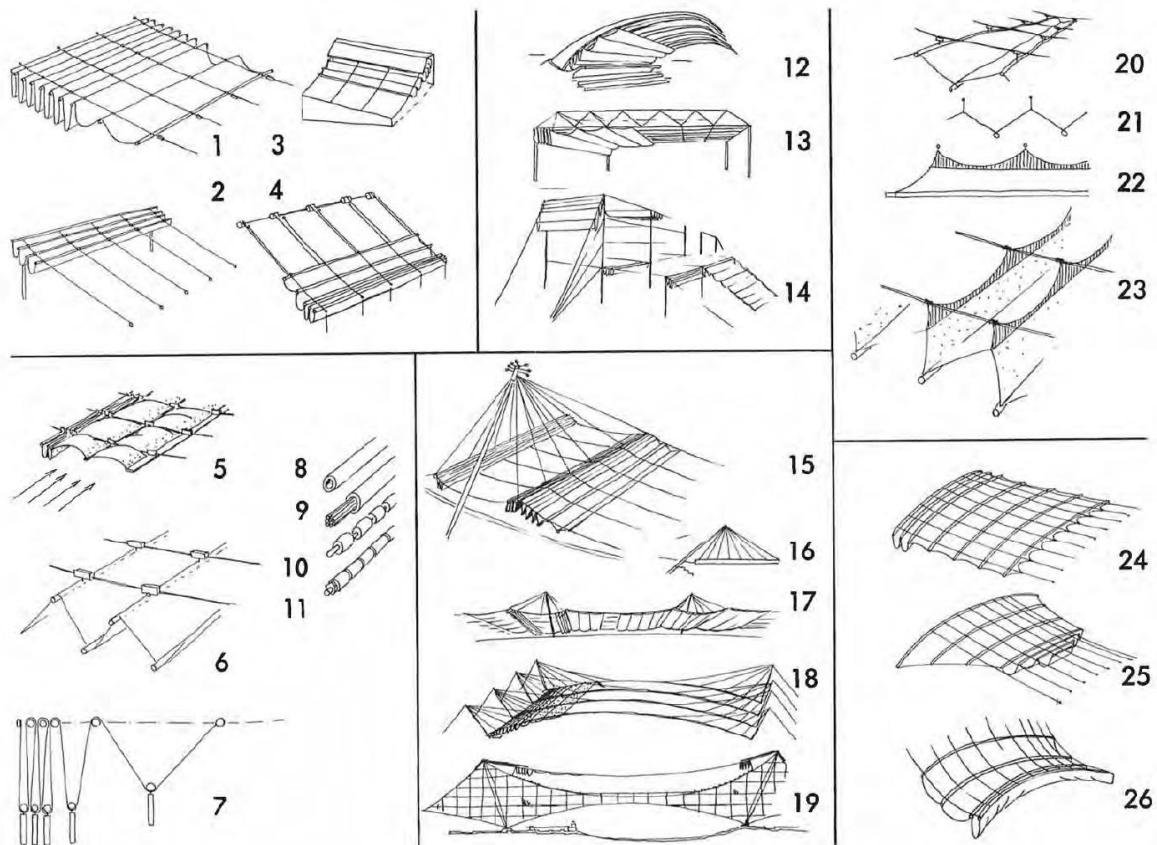


Figure 1: different types of toldo structures [3]

1.1 History and background

The idea of a convertible structure which can be adapted to changing weather condition is old. Various types of membrane constructions were built in the past centuries [15]. One of the oldest retractable shadings is umbrella. According to the written records, the oldest reference to a collapsible umbrella dates to the year around 45 BC which was design by Wang Mang in China [wiki]. However, based on the carved work of Persepolis in Persia (Iran) umbrellas were found repeatedly in some sculptures related to 550 to 330 BC [wiki].



Figure 2: umbrella designed by Wang Mang in china



Figure 3: umbrella in ancient Persia (Iran)

Apart from the umbrellas which are the one of the main type of the retractable fabric structures, toldo structures are in the interest of this research. Toldo shading structures are mostly known as flat retractable shading supported by cables and in some types suspended bending elements (like transoms or beams) with higher bending stiffness are used to direct the folding procedure. Colosseum arena in Rome could be one of the oldest structures which used to have toldo shading during the Roman Empire, in AD 80 [from internet research].



Figure 4: an imaginary image of Colosseum with toldo shading

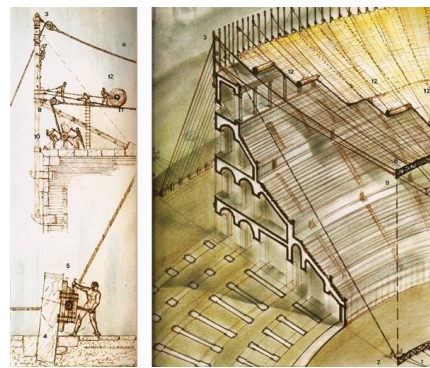


Figure 5: the retraction mechanism

The other type of the toldo shading systems can be found around Mediterranean during 16th century. The following Figure shows one of these system in Seville for funeral processions in the years 1570 to 1572 [IL5].

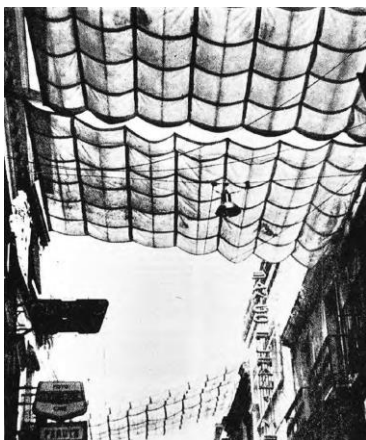


Figure 6: street toldo shading in Seville, Spain

After Frei Otto developed the theoretical principles of lightweight structures, the movement in this field speeded up and many tensile structures in different types and categories developed and executed. In the following Figures, some of significant toldo structures are introduced.

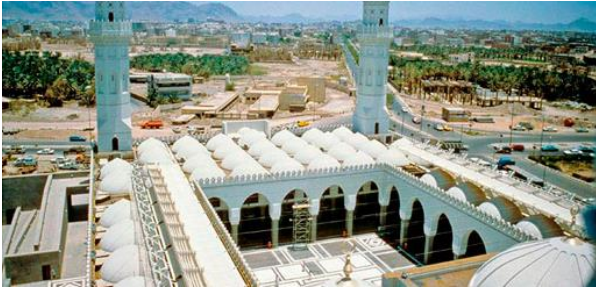


Figure 7: Quba Mosque toldo shading in retracted position, Madinah, KSA (SL Rasch, 1987)



Figure 8: Quba Mosque toldo shading in deployed position, Madinah, KSA (SL Rasch, 1987)



Figure 9: Commerzbank-Arena Frankfurt toldo shading in semi retracted position, Frankfurt, Germany (Schlaich Bergemann Partner, 2006)



Figure 10: Commerzbank-Arena Frankfurt in almost deployed position, Frankfurt, Germany (Schlaich Bergemann Partner, 2006)



Figure 11: the convertible membrane roof over the terrace of Villa D'Este, Rome, Italy (SL Rasch 1999)



Figure 12: Robinson club toldo shading in deployed position, Canary Island, Spain (SL Rasch, 1999)



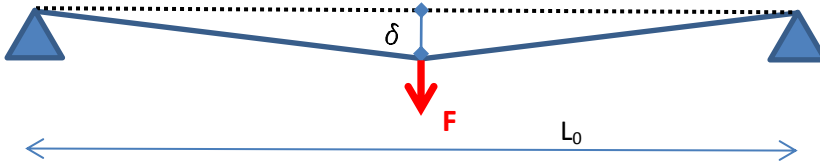
Figure 13: Robinson club toldo shading in deployed, Canary Island, Spain (SL Rasch, 1999)

As it is shown, this type of tensile structure is relatively flat with almost no curvature. This leads to nearly zero geometrical stiffness in this kind of shading skin. In the following sub-chapter (1.2), some structural concepts about the behavior of flat membrane structures are described.

1.2 Stiffness of the tensile membrane structures

Apart from in-plane tensile stiffness of the fabric membrane structures which is because of the fabric filament stiffness in warp and weft orientations, there is also out-of-plane stiffness which is perpendicular to the membrane face. The main reasons for such an out-of-plane behavior are (1) membrane pre-stress, (2) curvature and (3) in-plane stiffness of the membrane. The more membrane pre-stress, the less out-of-plane deformation means more stiffness. The more curvature, the more structural stiffness.

In order to illustrate these effects on the total out-of-plane stiffness of the membrane, the simply supported cable under a point load at the mid-span is considered as below.



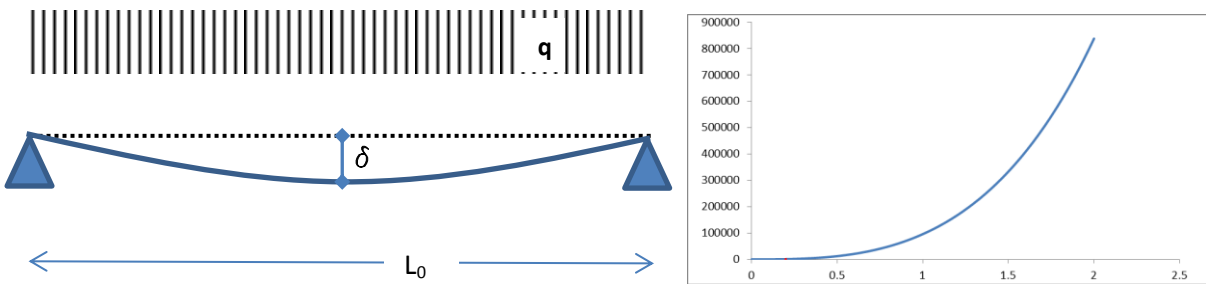
The initial length of the cable is assumed L_0 under the pre-tension of the P_0 and the deformed cable length under the point load (F) at the middle of the cable is considered as L carrying the tensile force of $P_0 + \Delta P$. Having $\frac{L}{2} \sin(\theta) = \delta$ and $F = 2(P_0 + \Delta P) \sin(\theta)$, the relation between load and vertical displacement at mid-span is obtained as

$$K = \frac{F}{\delta} = \frac{4}{L} (P_0 + \Delta P) \quad (1.1)$$

ΔP is specified based on the elongation of the cable which is $\Delta P = EA \left(\frac{L}{L_0} - 1 \right)$. Therefore, the stiffness could be presented as following relation:

$$K = \frac{F}{\delta} = \frac{4}{L} \left[P_0 + EA \left(\frac{L}{L_0} - 1 \right) \right] \quad (1.2)$$

As it is shown in the relation (1.2), the out-of-plane stiffness of the pre-tensioned cable is depending on pre-tension (P_0), axial stiffness of cable material and curvature $\left(\frac{L}{L_0} - 1 \right)$. The more $\left(\frac{L}{L_0} - 1 \right)$, the higher curvature. The same way can be applied for the uniform load on the cable. The final relation between the q and is presented in relation (1.3) which is illustrated graphically in the following Figure as well.



$$q = 2k \left[\sin^{-1} \left(\frac{4\delta}{L_0} \right) - \frac{4\delta}{L_0} \right] + \frac{2P_0}{L_0} \left(\frac{4\delta}{L_0} \right) \quad (1.3)$$

Based on the shown graph, by increasing the amount of initial sag (initial curvature), the stiffness of the system is also increasing. This shows the nonlinear behavior of the structure. As it is clear in the figure, the slope of the mentioned curve around the area with no initial sag is almost zero which means stiffness of the structure perpendicular to its length is nearly zero. This demonstrates the complex behavior of the flat tensile structures, especially under the dynamic loads. The structural behavior of pre-stressed flat membrane structures is studied in chapter 2. Similar concept can be stayed for all tensile membrane structures.

In conclusion, the stiffness of a tensile structure perpendicular to the alignment of the structure is depending on the mentioned factors and can be stayed as a function of them.

$$K_{total} = f\{K_{prestress}, K_{geometry}, K_{elasticity}\} \quad (1.4)$$

1.3 Dynamic simulation of prestressed membrane structures in the Literature

As it is described above, tensile structures as a prestressed flat tensile system are sensitive to the wind load and its dynamic effect. Hence, in the last decades different research studies have been performed on this topic mostly in the aerospace industry. However, in the field of tensile architecture, only a few research studies have been published. Some of the most relevant of them are introduced briefly here.

In 1972, Frei Otto and his research team have published “IL5 convertible roofs” at Institute of lightweight structure at Stuttgart University [3]. They explained different types of convertible roofs and their conceptual structural system. This comprehensive publication was the reference of different researchers and companies for several years. The dynamic effect of wind on membrane structure is studied by B. N. Sun, J. M. Wang and W. J. Lou in 2002. They could analytically investigate the effect of air mass on the membrane structure and derived the mathematical equation [8]. In 2004, the same researchers including J. M. Wang and B. N. Sun have investigated the effect of wind vortex on membrane structures under the unsteady wind flow [11]. They accomplished to verify their analytical results with the experimental test with a good correlation.

By improvement of computational tools and technologies in the last years, a group of researchers at Technical University of Munich (TUM) under the head of Prof. Dr.-Ing K.-U. Bletzinger started to develop a numerical methodology for wind structure interaction simulation specialized in tensile membrane structures. In 2007, Roland Wüchner, Alexander Kupzok and Kai-Uwe Bletzinger from TUM have developed a methodology to analyze the thin membrane-wind interaction problems [12]. Their proposed numerical solver could simulate the Fluid-Structure Interaction (FSI) of free form thin membrane under the wind load. Michalski et al. in 2011 have evaluated FSI numerical simulation with full scale experimental model [1]. They have built up a 29m span umbrella in real field and measured the structural responses of umbrellas in addition to wind speeds around the umbrella. Furthermore, they have set up a numerical model computing coupled CSD/CFD to evaluate the numerical structural responses by experimental model. The results showed that the FSI simulation is capable to be applied as an industrial design and engineering tool for the tensile structures.



Figure 14: Real scale setup of 29m umbrella in Liebherr, Germany

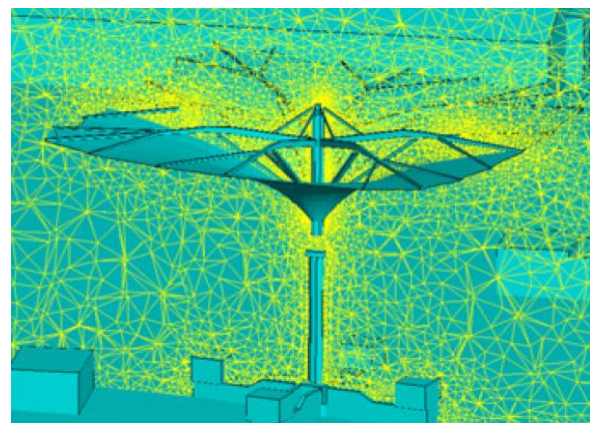


Figure 15: Real scale setup of 29m umbrella in Liebherr, Germany

Other research studies in the same area have been done by Michalski et al. on 53m umbrella in 2015 as a collaboration research by SL Rasch and ESI group [6] and on 29m umbrella which was led by H. Alsofi from the same research group at TUM [4]. He has evaluated the computational wind engineering tool with experimental results which were given by SL Rasch GmbH. Recent advances in computational wind engineering and fluid-structure interaction simulation have been reported by research and development team at SL rasch

GmbH in collaboration with R- Löhner from CFD center at George Mason University in USA and E. Haug from ESI group in France [6].

Although the air mass in most of the civil structures is ignorable, it matters when a thin lightweight membrane structure is moving in atmospheric environment. The more the membrane moves the air, the more effective the air mass is in the dynamic simulation of membrane structure under the wind flow. This effect even gets stronger when the membrane is made out of lightweight textile and has low curvature and prestress. In 2011, D. Sedlar et al. have investigated experimentally and numerically the effect of air added mass on thin cantilever beam which is submerged in water [9]. Y. Li et al. in 2011 have done a series of experimental and numerical studies for flat prestressed membrane vibrating in still air to estimate the amount of added mass [7]. They have derived a simple formula to estimate the air added mass. They have shown that the amount air added mass depends on membrane dimensions and air density and accordingly independent of the mode shapes.

2 Flat pre-stressed membrane structure¹

As it was explained in section 1.2, the load-deformation relation in tensile structure is not linear and the corresponding stiffness is depending on three main factors; (1) curvature, (2) pre-tension and (3) material stiffness. In this chapter, since the structure has no initial curvature, the behavior of the structure is investigated under two other factors. The static analysis is performed under uniform loading and dynamic free oscillation analysis to find first natural frequency of the structure. In order to reach to this goal, a **15.4×8 m** toldo is considered in this chapter. The structure consists of aluminum transoms, membrane and cables which is shown in the following figure. The membrane segments are supported by aluminum transoms (and supports and the end edges) and transoms are supported by steel cables and steel cables by the supports. The pre-tension for the membrane is fixed to **250 N/m**, but for the 3 supporting cables is different in various cases.

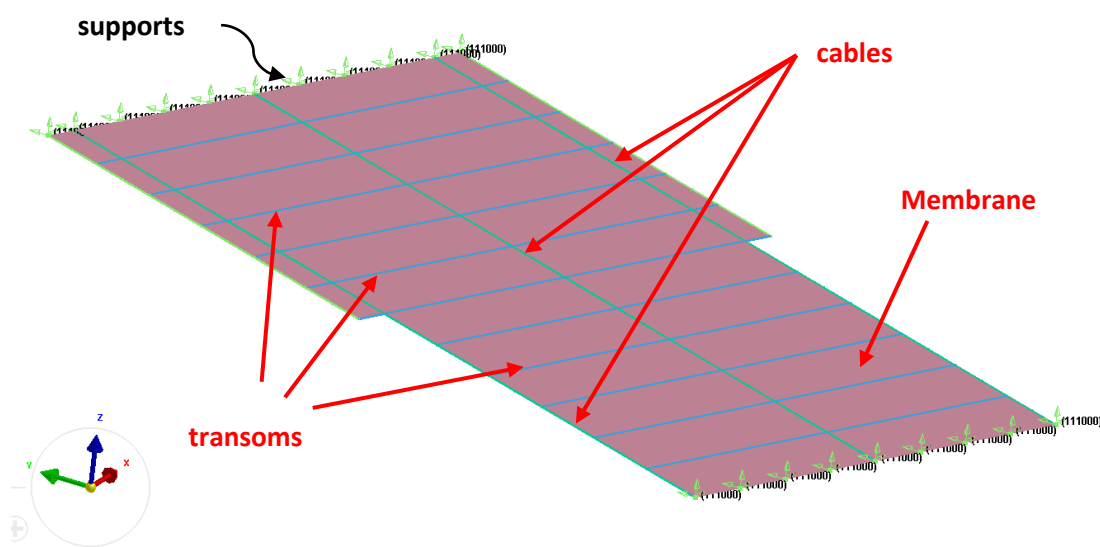


Figure 16: Structural system of the toldo

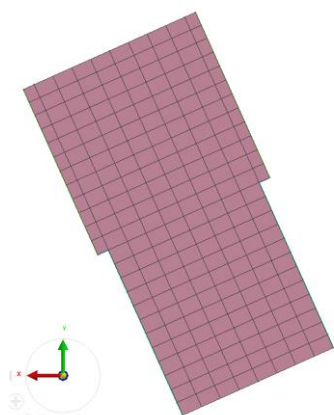


Figure 17: mesh size of the structural elements $0.5 \times 5.65 \text{ m}^2$

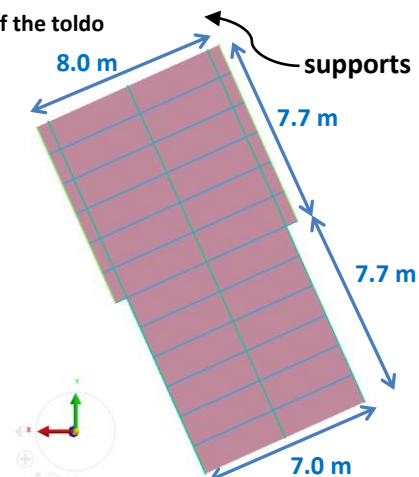


Figure 18: Dimensions

¹ In this study membrane structures means tensile membrane structures and there is no in-plane elasticity for the compressional actions.

In the following table, the information about the weight of each structural member is presented. The weight of the edge belt is negligible.

Structural member	Weight (kg)	The amount of participation in total mass (%)
Membrane	115.5	16 %
Steel cable	124.8	17.2 %
Aluminum transom	484.7	66.8 %
Total	725	100 %

2.1 The effect of pre-tension

As it is described in the previous sections, one of the parameters which affects the stiffness of the toldo structures is pre-tension. In order to consider this in more detail, a parametric study has been performed by applying different cable pre-tensions on the defined toldo in Figure (19). Loading is applied gradually to prevent any dynamic effect on the structural response.

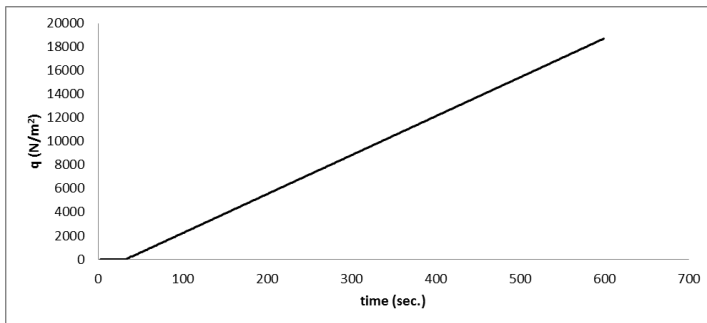


Figure 19: time history of the applied uniform load on the toldo membrane

In the following figure, the relation between the applied suction load and the displacement of the center point of the toldo for different cable pre-tensions are illustrated. In all the results the axial behavior of the membrane is tension-only and linear-elastic. The ratio of the membrane stress (N/m) to corresponding engineering strain (%) is 800'000 N/m.

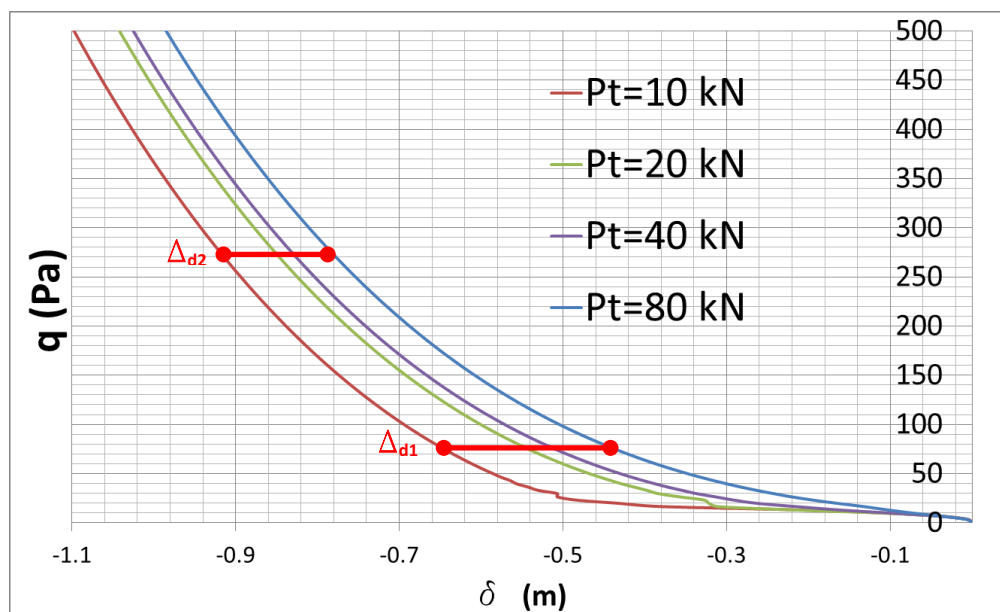


Figure 20: the relation between q and δ

Based on the result of the analysis shown in Figure (21) and (22), by increasing the cable pre-tension, for a given q (applied load), the governed displacement at the center of the toldo is reduced which means the growth of the stiffness of the structure. However, this growth is more significant in the lower range of applied force and in higher range is less. For example according to Figure (21), under the applied load $q=500\text{Pa}$, δ for cable pre-tension 10kN is about 1.7 times bigger than for the case with the cable pre-tension 80kN , but this ration tends to 1 for the higher amount of applied force. In the following graph the ratio of the displacement is shown versus the amount of cable pre-tension. Therefore, increasing the pre-tension in order to increase the structural stiffness or reduced the toldo displacement would not be effective enough higher than specific amount of applied load.

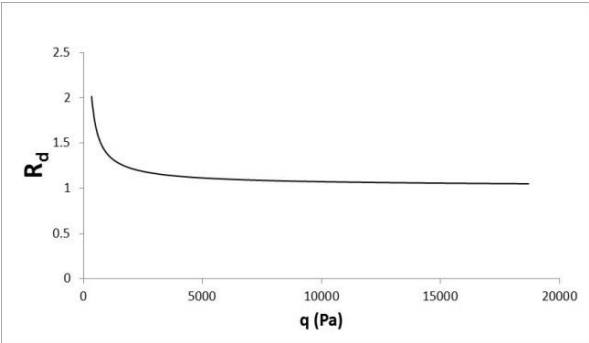


Figure 21: Displacement ratio (R_d) vs. applied load (q)

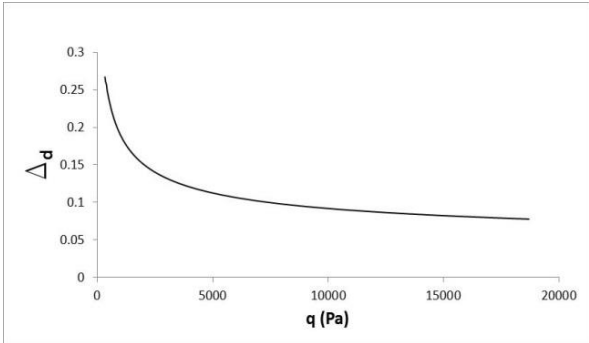


Figure 22: displacement difference (Δd) vs. applied load (q)

Minimum cable pre-tension

In order to define the cable pre-tension precisely, the form finding analysis with soap film elements have to be performed. If the form finding is done by considering the gravity, the initial sag would not be zero and the toldo gets belly, see figure (23). In this case, more attention is needed to define the cable-pre-tension, because if the amount of the pre-tension is too low, the tension in the cable might reach to zero when they get close to the flat position which causes an instable behavior in the structure for a moment, see figure (24, right). Therefore the amount of the pre-tension should be high enough to leave some tension when the toldo becomes flat. In contrary, if the gravity is not considered in the form finding step, it would be confident the tension in the cables does not go below than the defined pre-tension.

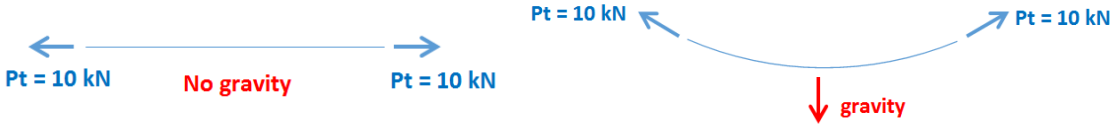


Figure 23: form finding phase – with soap film materials

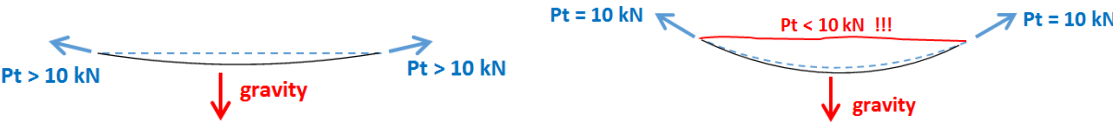


Figure 24: load analysis stage – with elastic materials

2.2 Eigen-frequency

The mentioned teldo is studied under release test to specify the natural first frequency of the structure. In order to investigate the effect of the pre-tension, a series of tests under different cable pre-tensions are performed. The following procedures are applied to the structure, see figures (25) and (26):

- Apply the gravity (g) in –Z direction to let the structure to get the pretension and/or form.
- Apply the acceleration uniformly on the structure in Z direction (against the gravity) and let the teldo to get blown up. The uniform acceleration lets the teldo to oscillate in its 1st mode shape.
- Keep the teldo in this position for a while to be sure that there is no vibration or dynamic noise in the structure.
- Release the structure from the applied acceleration to let it oscillate freely.

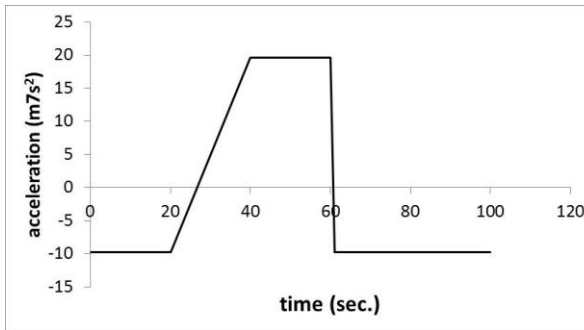


Figure 25: free oscillation with the gravity acceleration

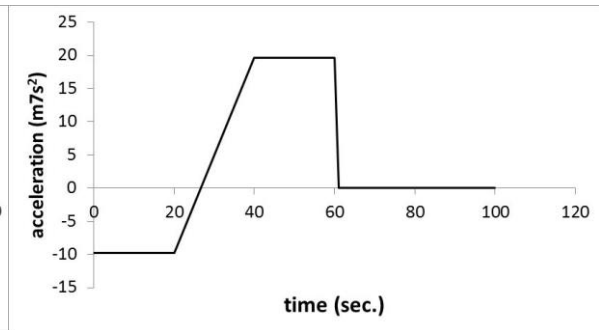


Figure 26: free oscillation without the gravity acceleration

In order to perform a proper free release test and achieve meaningful frequency, some issues should be taken into account.

- To avoid any dynamic effect during the stages 1, 2 and 3, some damping should be applied to the system in addition to the low rate of changing in acceleration. However, damping must be removed as the teldo is released to obtain natural frequency of the undamped system.
- The gravity must be considered in the analysis. In contrary to the most of the structures in which the gravity does not play any role in defining the natural frequency of the system, in pre-tensioned teldo structures gravity affects the natural frequency. The reason can be chased from the natural frequency of an undamped simply supported pre-tensioned cable (see Eq. 4). Based on the equation of the motion shown in the following Eq. (1), the first natural frequency of the system can be governed as below:

$$m \frac{\partial^2 u}{\partial t^2} - N \frac{\partial^2 u}{\partial x^2} = mg \quad \text{Equation 1}$$

In which the m is the mass of the cable per length, N is the cable pretension, u is the displacement of the cable perpendicular to the cable alignment and x is the component of the spatial location along the cable from one end. By assuming the following expansion for the u , the Eq. (1) can be coupled as Eq. (2)

$$u(x, t) = \sum_{i=0}^{\infty} a_i \sin\left(i \frac{\pi}{l} x\right) \overbrace{\sin(\omega_i t)}^{q_i(t)} \quad \text{Equation 2}$$

$$\ddot{q}_i(t) + \frac{N}{m} \left(\frac{i\pi}{l} \right)^2 q_i(t) = \frac{\sqrt{2ml}}{i\pi} g [1 - \cos(i\pi)] \quad \text{Equation 3}$$

In which $\frac{N}{m} \left(\frac{i\pi}{l} \right)^2$ is equal to eigen-frequency of the system for mode i^{th} . Therefore, The angular frequency of the 1st mode is

$$\omega_1 = \frac{\pi}{l} \sqrt{\frac{N}{m}} \quad \text{Equation 4}$$

As it is shown from Eq. (4), by increasing the cable force the natural frequency of the structure is increased as well. This exactly happens when the gravity is applied in the free oscillation analysis and leads to rise of tensile force average in the cable. In this case the cable vibrating around the new position which is curved and more elongated comparing to the flat position.



The numerical results of the mentioned toldo system under different cable pretensions introduced in the section (2) are compared for the two cases (1) under gravity and (2) without gravity and presented in the Fig. (27) to (30). Pt stands for pretension force.

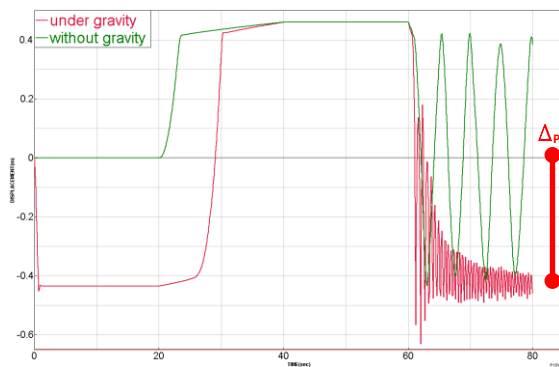


Figure 27: displacement of the center of the toldo in time – Pt =10 kN

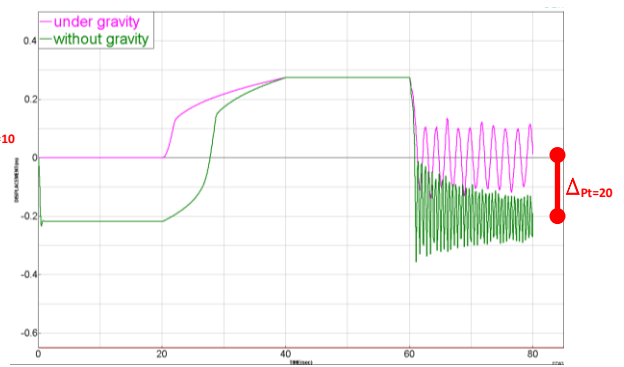


Figure 28: displacement of the center of the toldo in time – Pt =20 kN

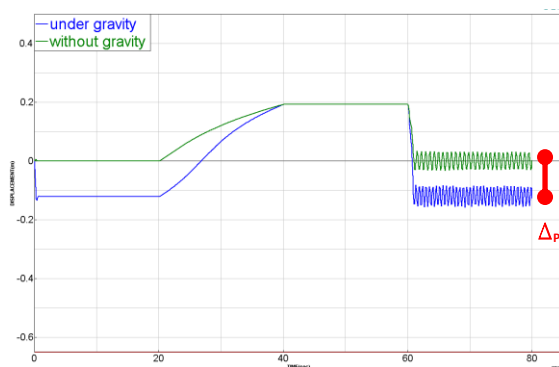


Figure 29: displacement of the center of the toldo in time – Pt =40 kN

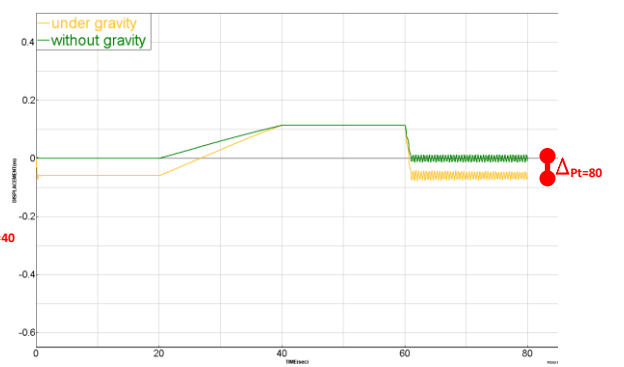


Figure 30: displacement of the center of the toldo in time – Pt =80 kN

As it is clear from the comparison of the oscillation of the toldo center, having no gravity reduces the natural frequency of the first mode which is because of the reduction of average tensile force in the cables during the oscillation. This difference gets lower when the cable pretension is set to higher values. The reason is by increasing the cable pretension, the sag of the toldo under the gravity would be smaller than the cases with lower pretensions, therefore the average of the tensile cable force during the oscillation for both cases of “under gravity” and “without gravity” would be close to each other, look at the Δ in the Figs. (27) to (30).

$$\Delta_{Pt=10} > \Delta_{Pt=20} > \Delta_{Pt=40} > \Delta_{Pt=80}$$

Additionally, according to the Fig. (31) to (34), the behavior of the toldo under the gravity shows a kind of attenuation during the oscillation although no damping is active after toldo gets released. This can be explained by performing Fast Fourier Transform (FFT). As it is shown in the following figures, the effect of 2nd natural mode (or in general higher modes) in cases Pt = 10kN and Pt = 20kN are not ignorable and they actively cancel the effect of the 1st mode during the oscillation.

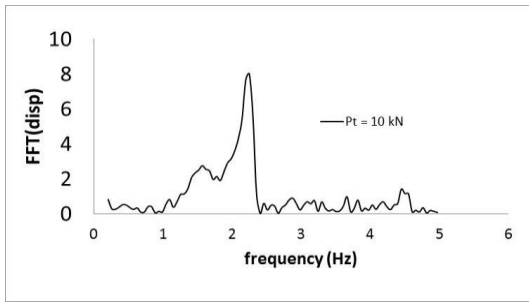


Figure 31: Response spectrum – Pt =10 kN

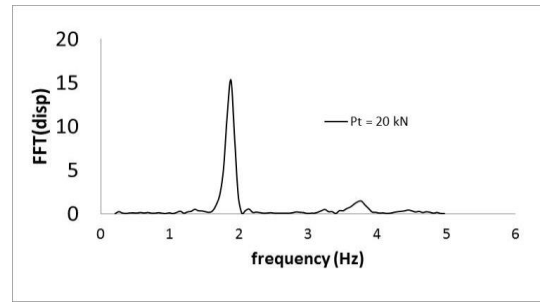


Figure 32: Response spectrum – Pt =20 kN

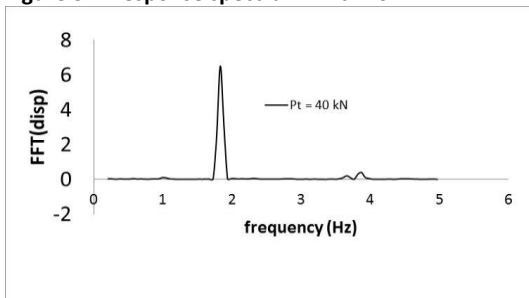


Figure 33: Response spectrum – Pt =40 kN

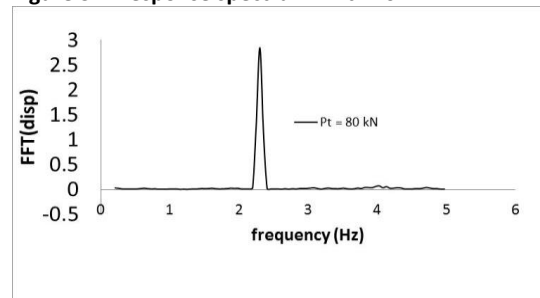


Figure 34: Response spectrum – Pt =80 kN

It should be noted that the behavior of the structural system in this study is nonlinear. Therefore, the result of the performed nonlinear FFT would be approximate. However, to investigate the effect of the cable pretension on the participation of the higher modes in free oscillation study would be acceptable.

- iii. The other effective parameter to perform a meaningful free oscillation analysis is the amount of the inverted acceleration which is applied to blow up the toldo. The amplitude of the release should be in a range that the toldo is supposed to vibrate under the given wind flow. However the sensitivity of the frequency to this factor has been studied and the results are shown in the following figures.

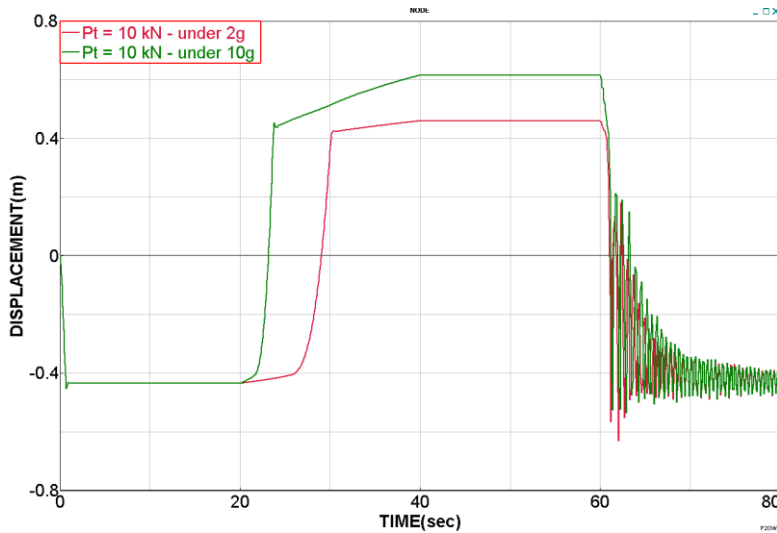


Figure 35: displacement of the center of the toldo in time – Pt =10 kN (a) under the 2g in red (b) under the 10g in green

The result shows that the time periods of the first five local peaks of toldo under 2g and 10g are 0.7 and 0.66 second respectively which gives the difference of 6% and by increasing the cable pretension this difference even reduces more. Therefore, the amount of blowing up acceleration does not affect the frequency of the system significantly.

- iv. It would be quite important how to measure the time period, because the interval of peaks is changing in time. For example, for the toldo under the cable pretension of 10kN, the time period measured from the first two peaks (0.7 sec.) is 1.75 times bigger than the time period gained from 16th and 17th (0.4 sec.), see Fig. (36) and (37). The reason can be explained by the amount of the cable force average which is less at the beginning of the oscillation. The reason is the lower amount of cable pretension which results in zero tension when the toldo reaches the flat position. However, by increasing the pretension the time period is almost constant during the free oscillation.

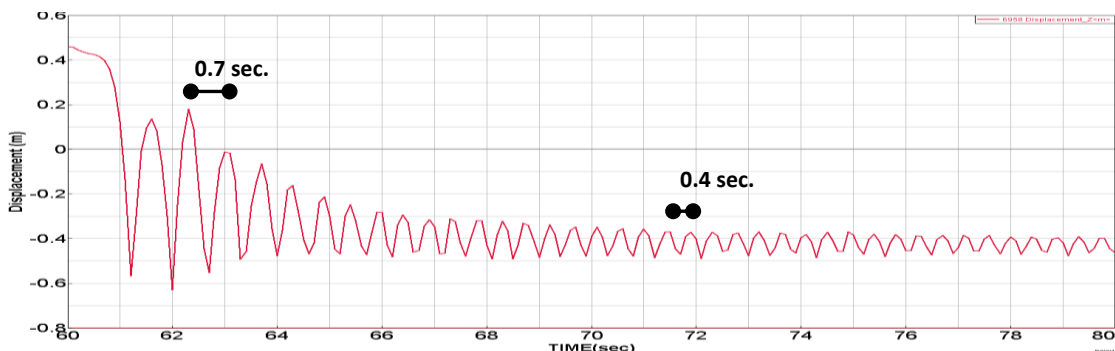


Figure 36: displacement of the center of the toldo in time – Pt =10 kN

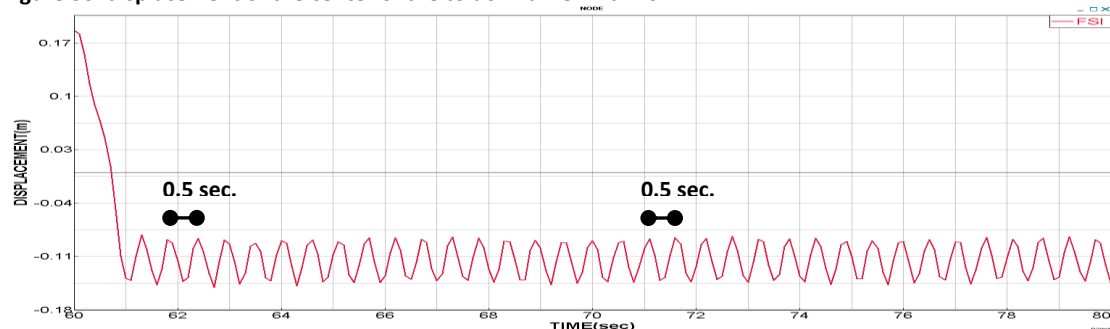


Figure 37: displacement of the center of the toldo in time – Pt =40 kN

2.2.1 Frequency - Pretension

As it is discussed so far, the cable pre-tension plays an important role in dynamic behavior of the tordo structures. By increasing the total pretension of the structure (cable pretension and membrane prestress), the eigen-frequency is increased and the behavior of the structure tends to linear behavior.

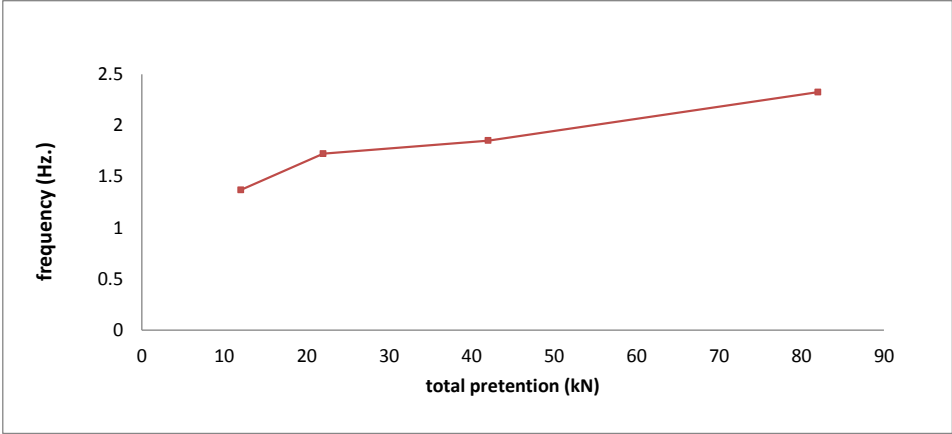


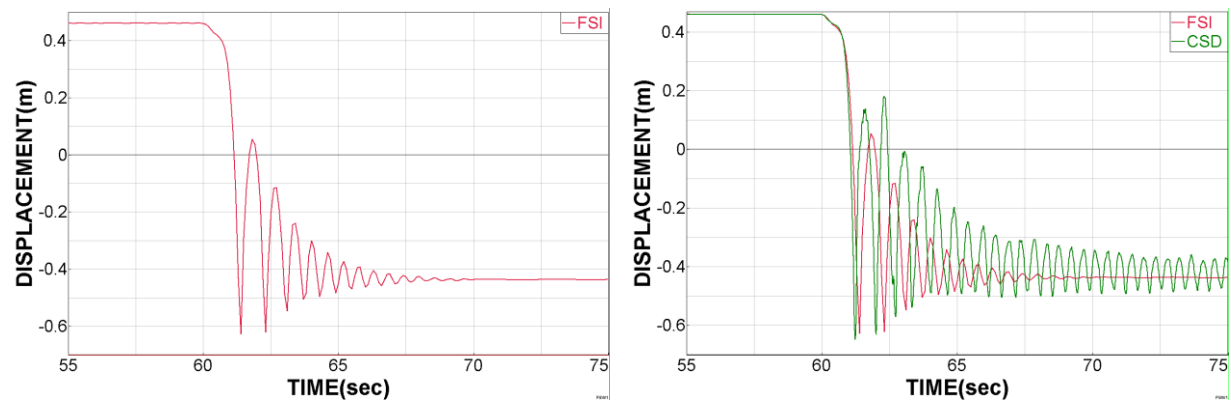
Figure 38: first natural frequency by changing the total pretension of the structure

3 The Aero-dynamic effect on the dynamic characteristic of toldo

The interaction between membrane structures and the environment has non-negligible effect on the structural response as the membrane moves the surrounding air more. This makes the mass of the moving air comparable with the ultra-lightweight membrane skin as the air stiffness and air damping (aerodynamic damping). In order to consider this effect in numerical simulation, Fluid Structure Interaction (FSI) simulation is needed to couple the CSD-modeled membrane structure with CFD-modeled air.

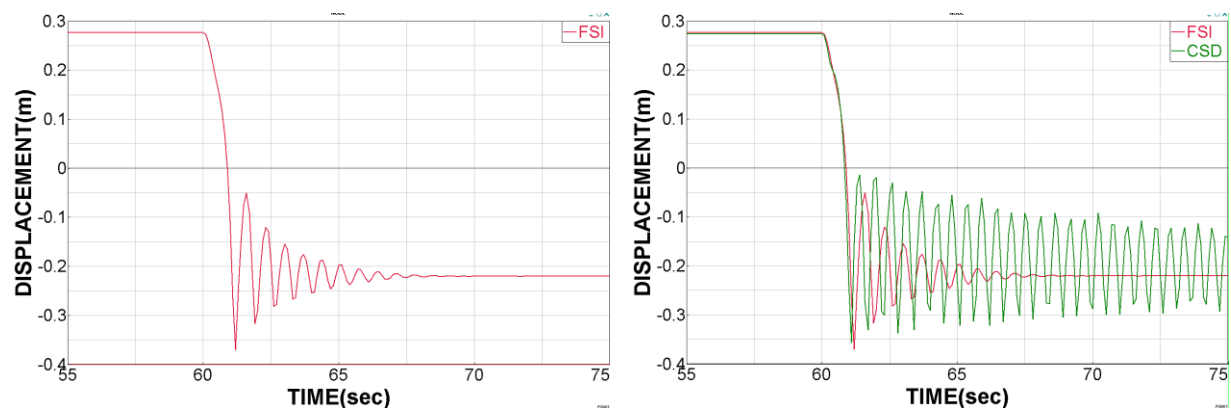
3.1 Free Oscillation

In the following figures the results of free release of the toldo structure in the still air are presented. FSI simulation is performed to capture the effect of the surrounding air. The CFD environment is limited by wall boundary in 5m beneath the toldo to consider the effect of the floor below the toldo membrane.



(a) (b)
Figure 39: time history of displacement of the toldo center node – Pt =10 kN (a) FSI simulation (b) FSI in comparison with CSD simulation

Sa



(a) (b)
Figure 40: time history of displacement of the toldo center node – Pt =20 kN (a) FSI simulation (b) FSI in comparison with CSD simulation

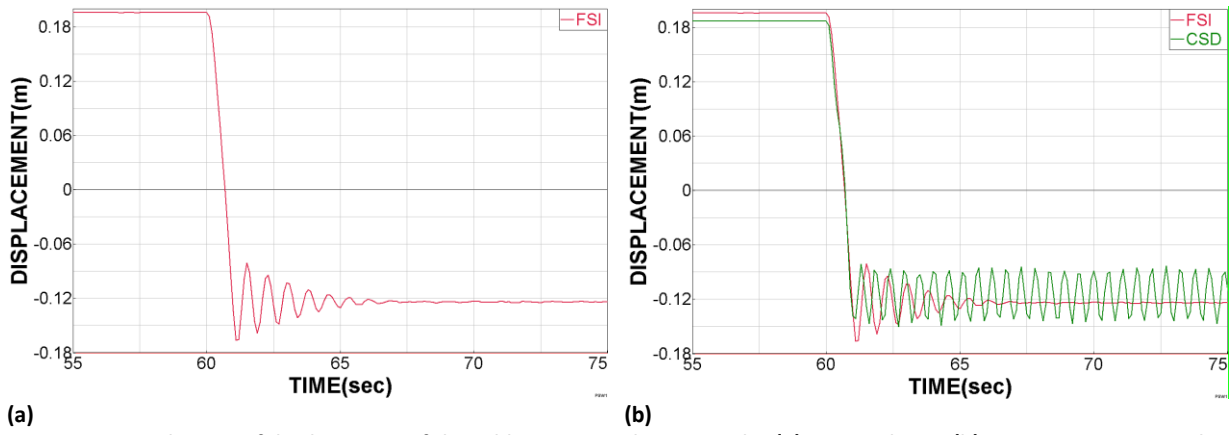


Figure 41: time history of displacement of the toldo center node – Pt =40 kN (a) FSI simulation (b) FSI in comparison with CSD simulation

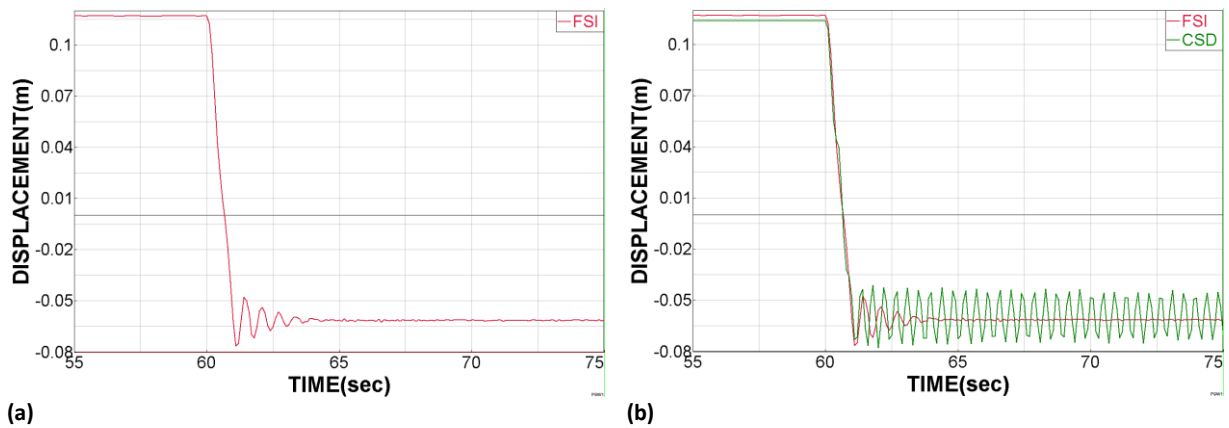


Figure 42: time history of displacement of the toldo center node – Pt =80 kN (a) FSI simulation (b) FSI in comparison with CSD simulation

As the results of FSI and CSD simulations are compared in the following table, by decreasing the cable pretension, the structural response of toldo in CSD is getting closer to FSI simulation.

Cable pretension (kN)	Time period (sec.)		Increasing proportion
	FSI simulation	CSD simulation	
10	0.73	0.73	1.01
20	0.71	0.58	1.23
40	0.76	0.54	1.41
80	0.65	0.43	1.50

3.1.1 Definition of the added mass and aerodynamic damping

In order to measure the amount of air mass, the following equations are derived from the basic relation of natural time period for a linear structural system. The effect of the air stiffness is ignored according to free space in the CFD model for air movement.

$$T = 2\pi \sqrt{\frac{m}{k}} \quad \text{Equation 5}$$

By dividing corresponding formula in FSI case to CSD case:

$$\left(\frac{T_{FSI}}{T_{CSD}}\right)^2 = \frac{m_{FSI}/k_{FSI}}{m_{CSD}/k_{CSD}} \quad \text{Equation 6}$$

By assuming $k_{FSI} = k_{CSD}$ and $m_{FSI} = m_{CSD} + m_{air}$, the Eq. (6) can be rewritten as

$$\frac{m_{air}}{m_{CSD}} = \left(\frac{T_{FSI}}{T_{CSD}}\right)^2 - 1 \quad \text{Equation 7}$$

In the following table the added air mass and aerodynamic damping for each cable pretension are presented. The aerodynamic damping is obtained from the damping decrement of free oscillation response.

Cable pretension (kN)	Time period (sec.)		Increasing proportion	m_{air}/m_{CSD}	m_{air} (kg)	Damping ratio $\zeta = \delta / 2\pi$		
	FSI simulation	CSD simulation				Peaks 1 to 5	Peaks 1 to 3	Peaks 3 to 5
10	0.73	0.73	1.01	0.02	13.4	0.065	0.073	0.057
20	0.71	0.58	1.23	0.50	363.7	0.068	0.076	0.061
40	0.76	0.54	1.41	1.00	723.7	0.067	0.057	0.077
80	0.65	0.43	1.50	1.25	906.3	0.102	0.084	0.121

Y. Li et al. have presented for air added mass the following formula which is independent of the eigen-frequency and depends on the membrane geometry and air density.

$$M_a = 0.68 \rho l \quad \text{Equation 8}$$

l is the diameter of the inscribed circle on the membrane face and M_a is the added air mass per unit area of the membrane. In this expression, air added mass is constant for a given geometry and does not change as cable pretension alters. The mentioned formula left around 730 Kg for the total air mass which is close to only the result of the toldo under the 40 kN cable pretension. The disagreement of other cases can be because of their mode shapes which are affecting the movement of free oscillation test.

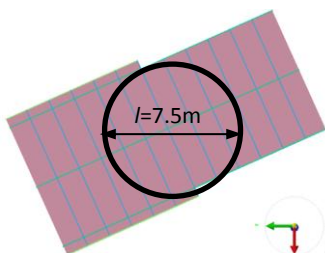


Figure 43: inscribed circle to the toldo face

3.2 Calibration of CSD model corresponding to FSI

In order to reduce the cost of the FSI simulation (like duration and the number of used CPUs), the air mass and structural damping of the CSD model is calibrated in order to avoid costly CFD simulation but keep the effect of air mass and aerodynamic damping in the same time.

The results show strong agreement between FSI simulation and calibrated CSD simulation in free oscillation study under different cable pretensions.

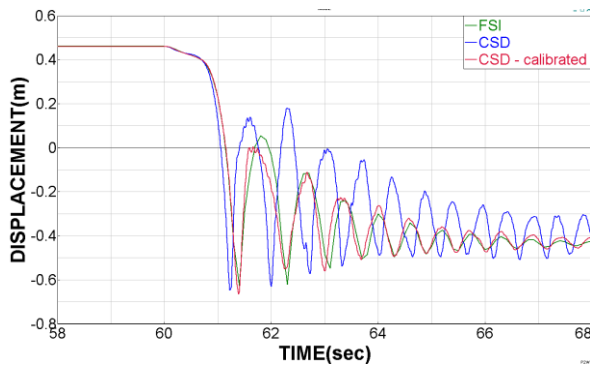


Figure 44: displacement of toledo center under free release – Pt =10 kN

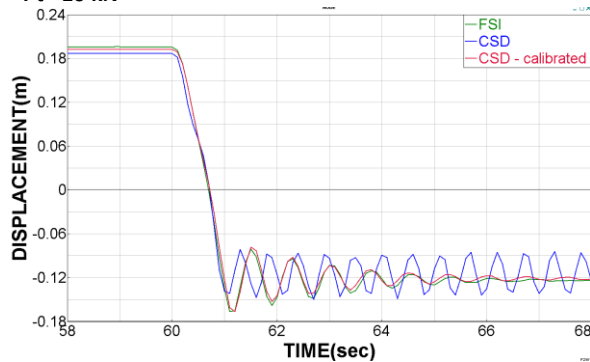


Figure 46: displacement of toledo center under free release – Pt =40 kN

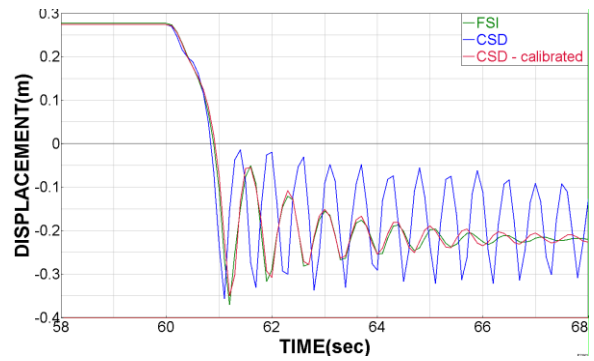


Figure 45: displacement of toledo center under free release – Pt =20 kN

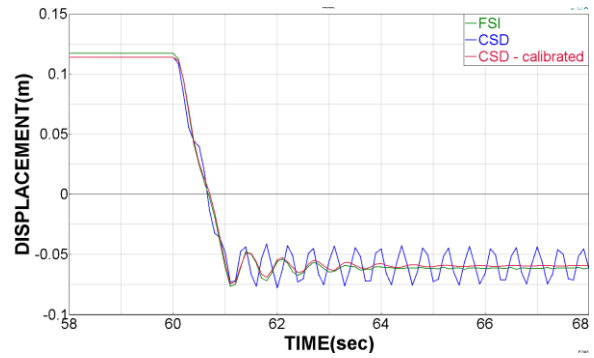


Figure 47: displacement of toledo center under free release – Pt =80 kN

4 Wind simulation

4.1 Design wind speed for convertible toldo structures

The design wind speed for the considered area is determined to be 50m/s (3s gust, 50m height, recurrence period of 50 years) resulting from the cite specific wind specialist study for that region by Davenport Wind Engineering Group.

The convertibility of the proposed shading system allows the truncation of extreme wind loading with a small probability of occurrence. As a design base, the ventilated toldo structure shall resist a maximum gust wind speed in shading position of 35 m/s (instead of 50m/s). The equivalent 10 minutes average is approx. 22m/s. The mechanical system has to be designed to guarantee the operation of the toldos in combination with an installed wind speed measurement system up to a mean wind speed of 15 m/s.

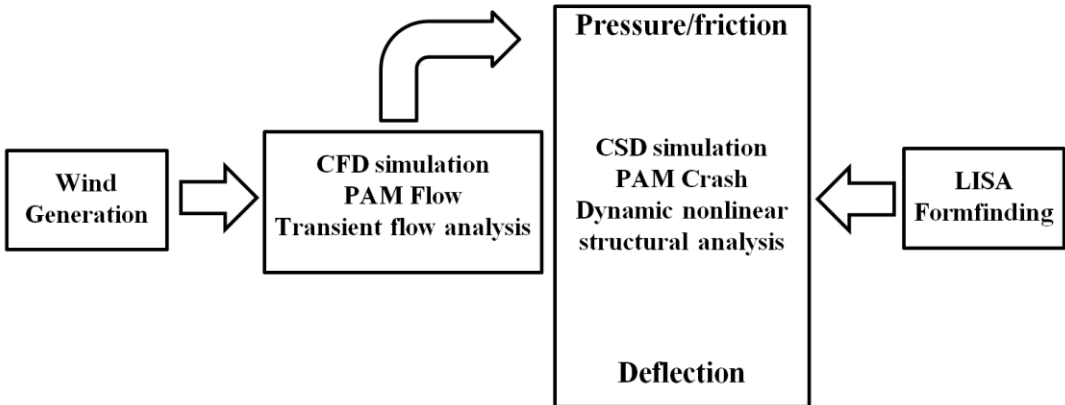
At higher wind speeds the convertible toldo has to be in its closed position or other devices have to be applied to reduce the wind loads on the supporting structure

Reference gust wind speed of 35 m/s is considered on the eaves height of the structure. Therefore the stagnation pressure results to $q = 0.8 \text{ kN/m}^2$.

4.2 CSD simulation

In this part the CSD simulation is performed under the wind pressure time series which is governed from CFD analysis. It means once in CFD environment, the wind flow is applied on the rigid flat toldo without considering the elasticity of the structure to get the air pressure close to the toldo (top and bottom) and then the governed air pressure is applied on the elastic toldo in CSD environment to get the structural responses. The main differences of this method with the real physics are:

- 1) Wind pressure is independent of the membrane deformation the toldo.
- 2) The estimated applied nodal aero-dynamic damping cannot be modelled.
- 3) The effect of air stiffness is not considered in the simulation.



4.2.1 CFD simulation

The CFD wind simulation is performed in the following environment. The solver is pamflow from ESI group. The specification of the CFD model is described in the following table.

Table 1: Physical and control parameters used for the CFD simulations

Solver Settings	
Transient	Yes
Number of Stages for Runge Kutta	5
CFL	1.0-1.3
Time Step	4 -7 ms
Pressure Algorithm Settings	
Type	QUICK
No. of pressure solving iterations	500
Relative Tolerance	0.001
Absolute Tolerance	1.0E-06
Weak Compressibility	Yes
Fluid Properties	
Fluid	Incompressible Fluid
Density	1.2 kg/m ³
Viscosity	1.8E-05 Pa – s
Turbulence Properties	
Turbulence Model	LES with SGS
Length Scale	0.0
Smagorinsky Constant	0.10
Y+ Distance for wall function	0.01

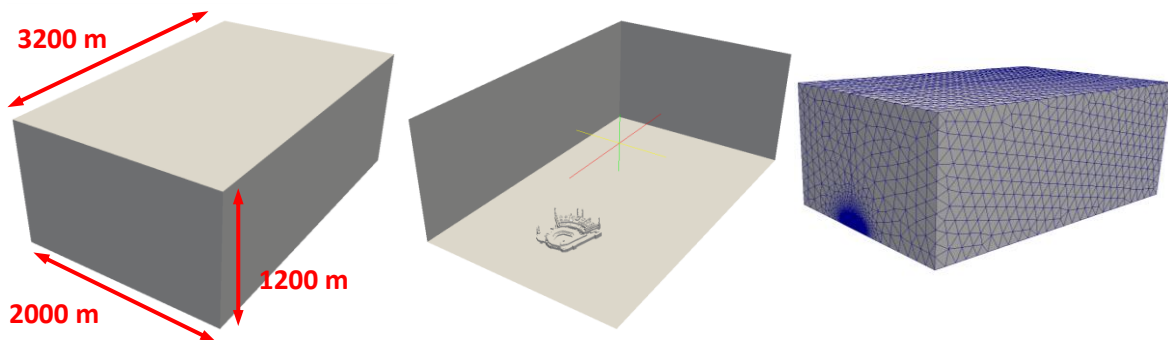


Figure 48: dimension of the CFD environment

In order to determine pressure coefficient (C_p) from CFD environment, wind pressure of 8 probes on 4 different positions on top and bottom of the membrane are measured. Therefore, the deviation of the obtained pressures at each position is scaled by the reference pressure which is 0.727 kPa. The ensemble averaging is applied on four different time series to estimate a unique time series for C_p which is uniformly distributed over the toldo.

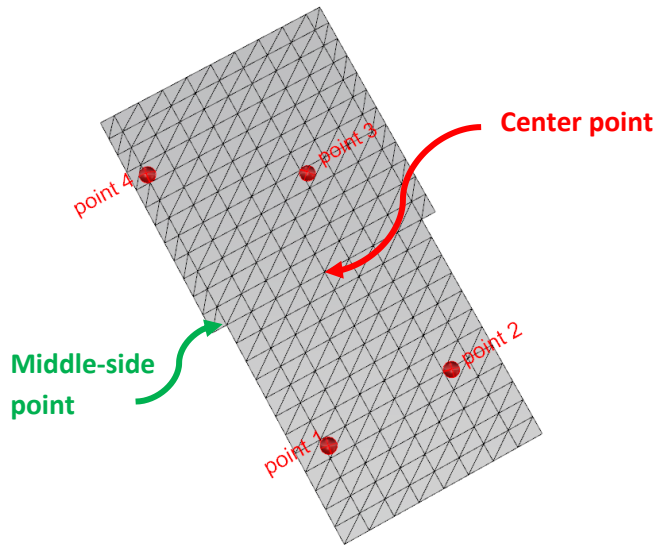


Figure 49: measuring points around the toldo in CFD environment

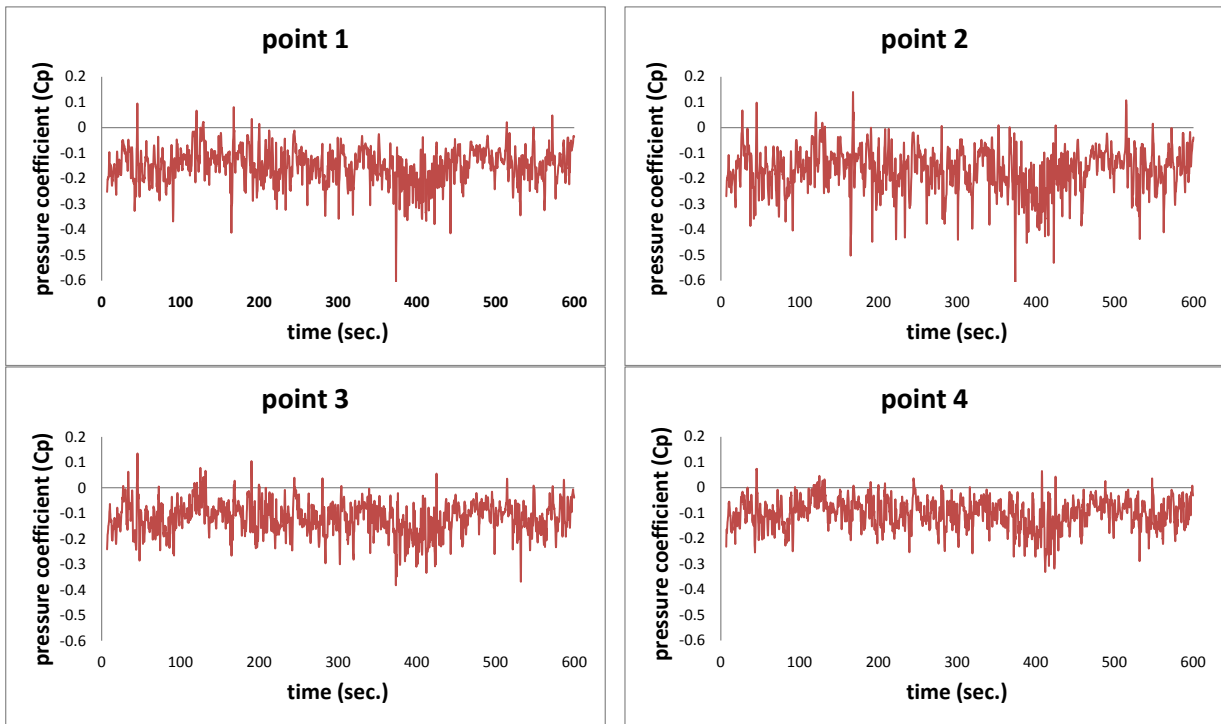


Figure 50: time history of air pressure coefficient factor for four different points of the toldo from CFD wind flow simulation

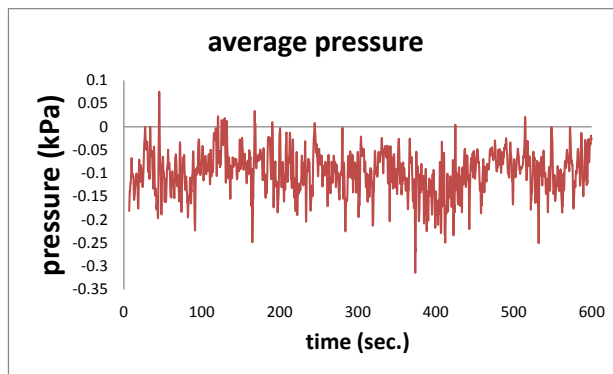


Figure 51: time history of average air pressure of the toldo from CFD wind flow simulation

4.2.2 CSD simulation

CSD simulation is done by an explicit solver which is called pamcrash from ESI group. This code is able to solve the large deformed structural problem. Therefore, it is suitable for modelling the mentioned pre-stressed membrane which is experiencing large movements.

In this part the calculated average air pressure from CFD analysis is applied uniformly on the toldo structure and solved as an elastic system in a CSD simulation. A parametric study performed to investigate the effect of cable pretension on the structural response of the toldo.

As it is shown in the following figures, by increasing the cable pretension the maximum deformation of the toldo and the standard deviation of all structural responses (like deformation and cable force) are decreased. However, this is not the same case for cable force. The minimum cable reaction occurs under the 40kN cable pretension and the maximum under the 80kN. This means there is an optimum cable pretension that leads into lowest maximum cable force.

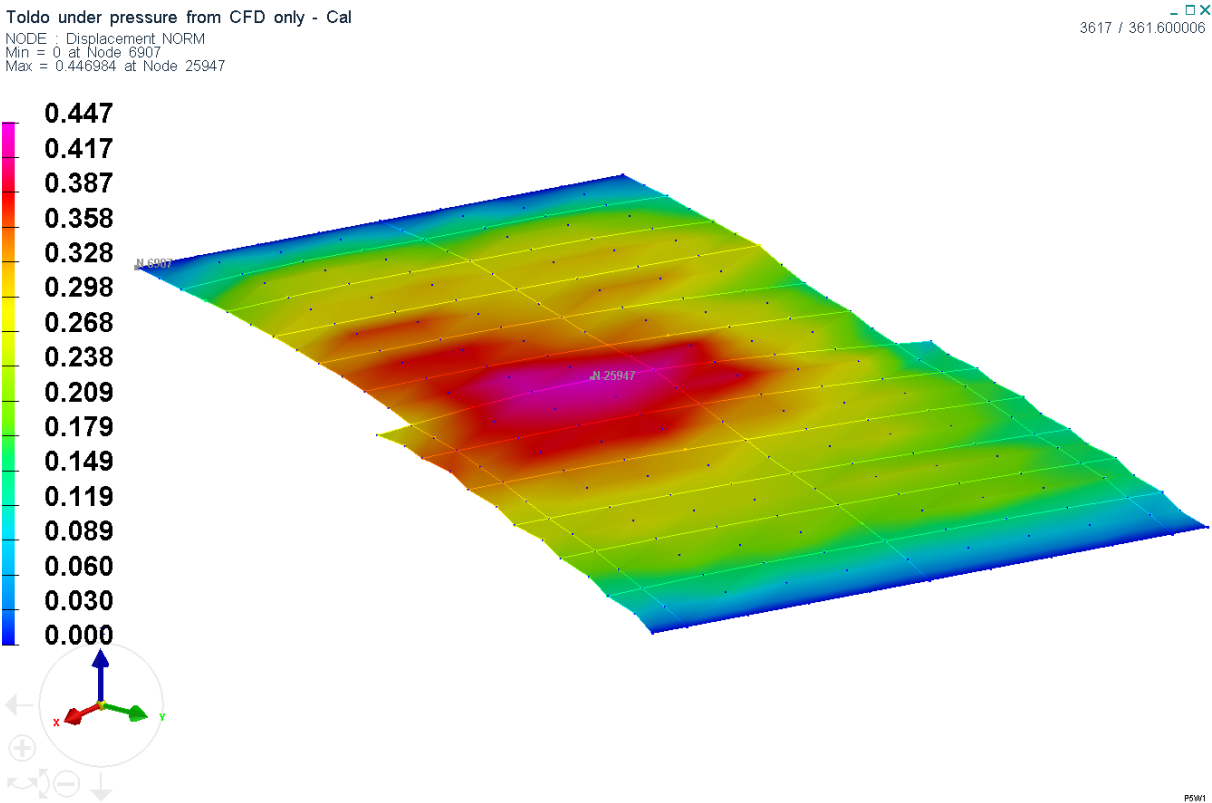


Figure 52: displacement contour of CSD model under the pressure loads extracted from separate CFD simulation

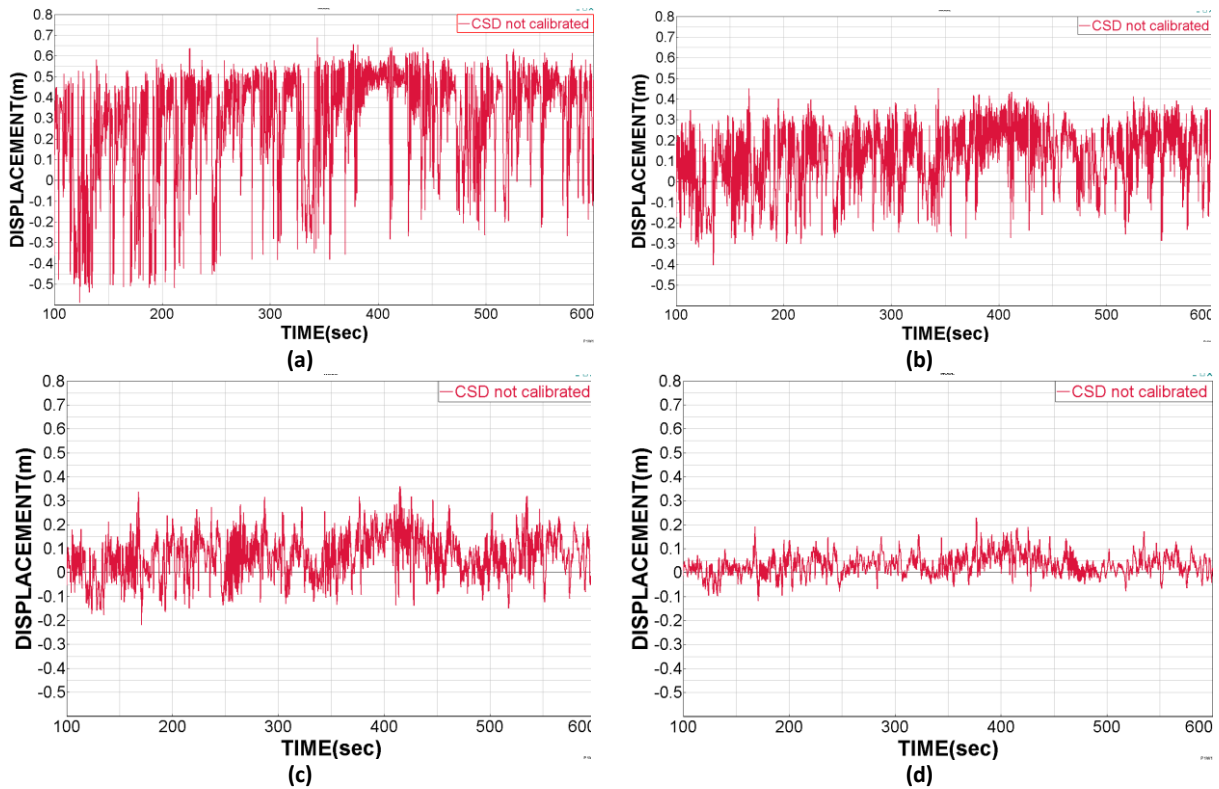


Figure 53: time history of displacement of the toldo at center point – CSD simulation (a) Pt = 10 kN, (b) Pt = 20 kN, (c) Pt = 40 kN and (d) Pt =80 kN

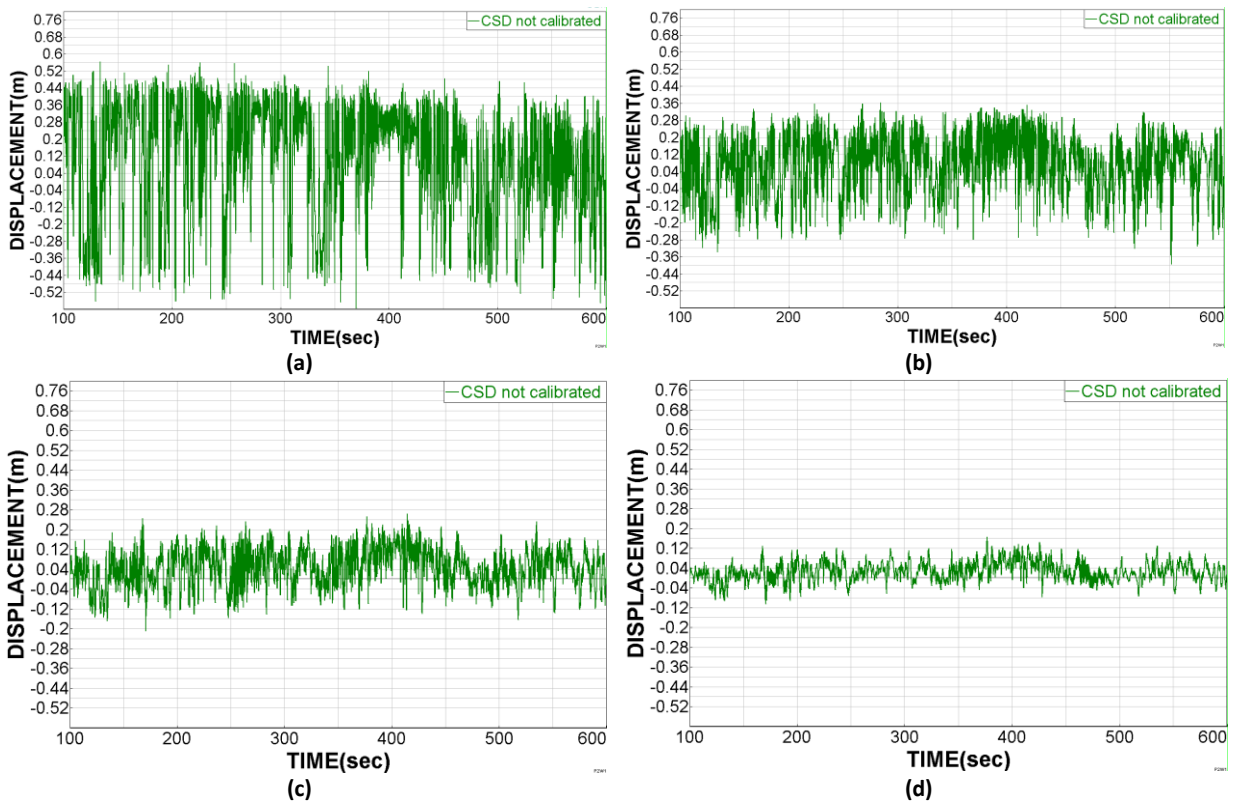


Figure 54: time history of displacement of the toldo at middle-side point– CSD simulation (a) Pt = 10 kN, (b) Pt = 20 kN, (c) Pt = 40 kN and (d) Pt =80 kN

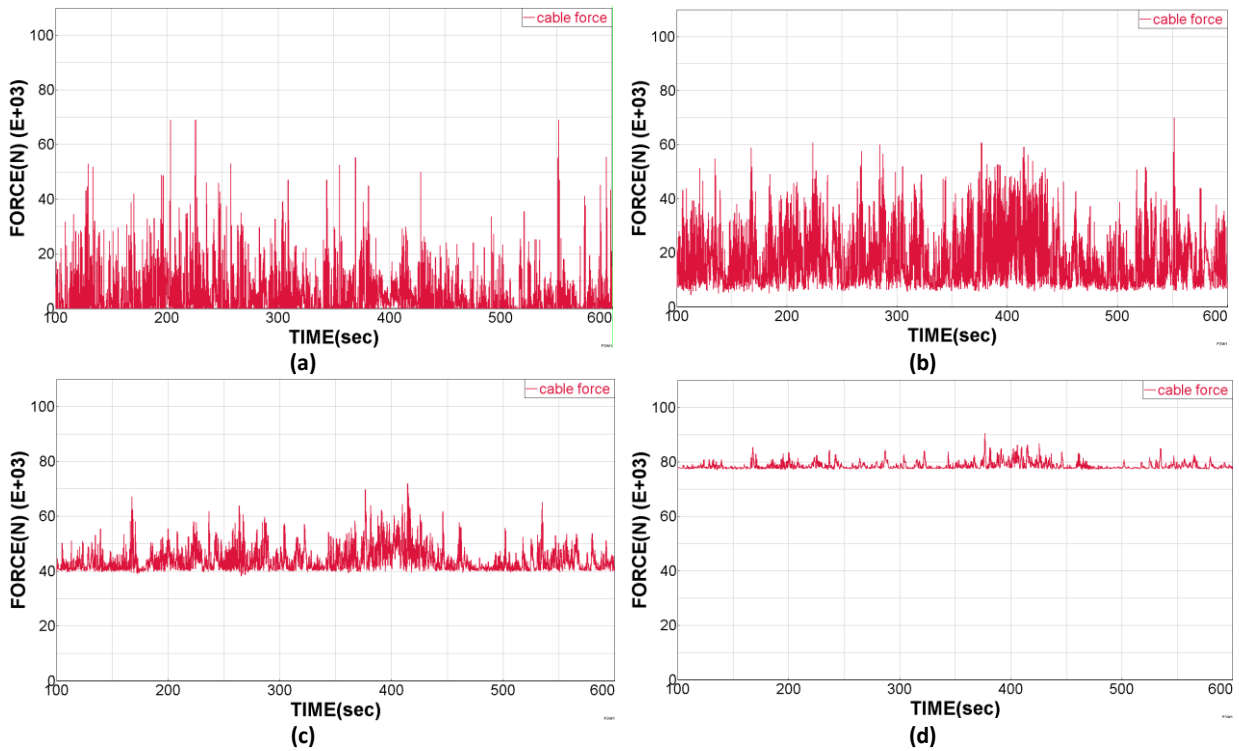


Figure 55: time history of middle cable force– CSD simulation (a) Pt = 10kN, (b) Pt = 20kN, (c) Pt = 40kN and (d) Pt =80kN

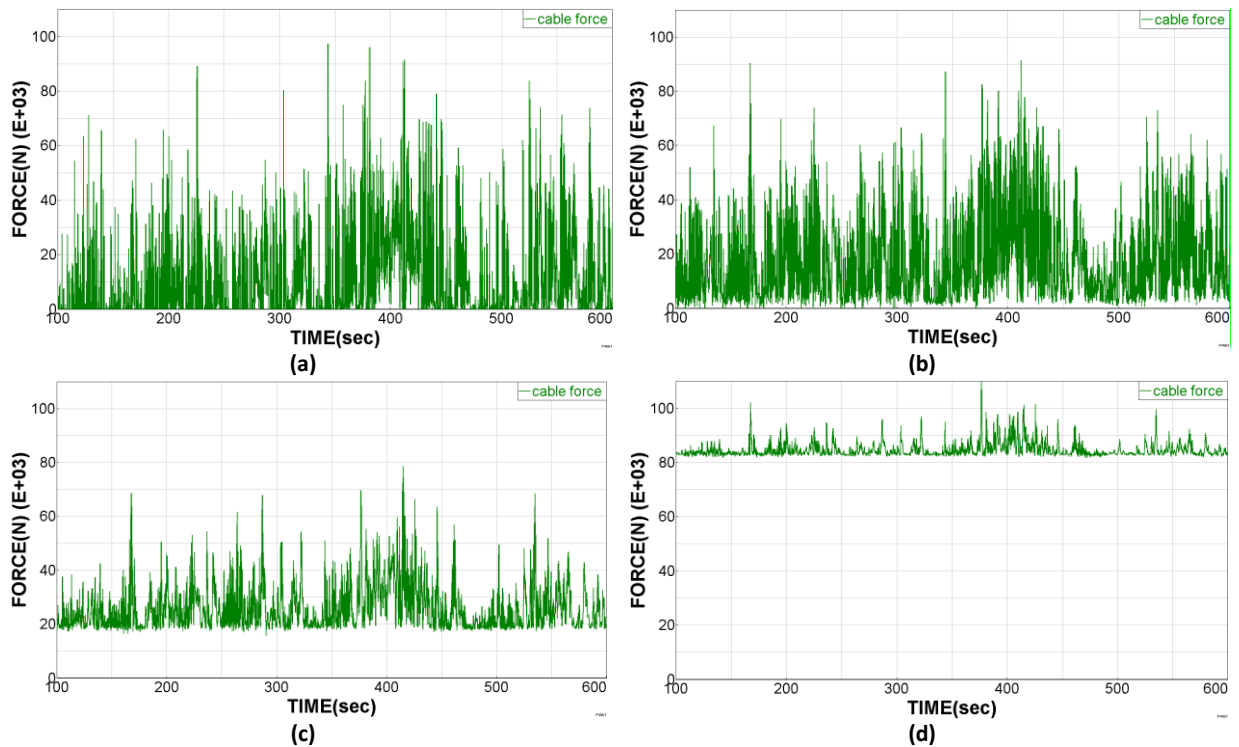


Figure 56: time history of side cable force– CSD simulation (a) Pt = 10 kN, (b) Pt = 20 kN, (c) Pt = 40 kN and (d) Pt =80 kN

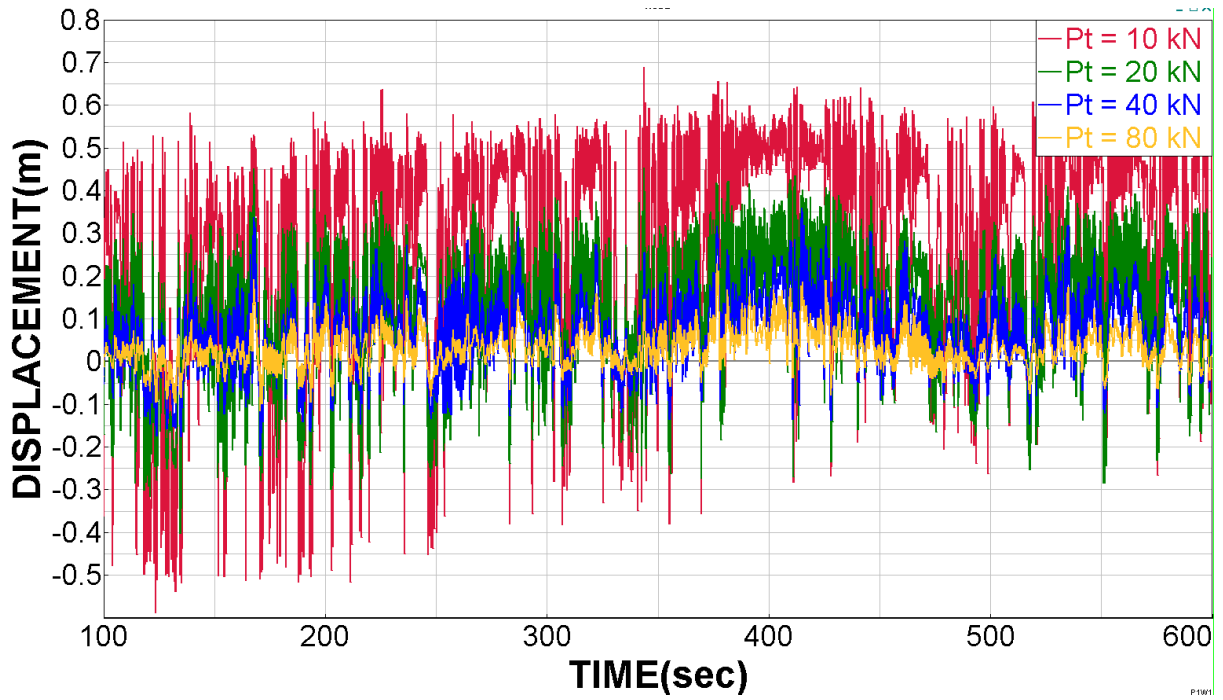


Figure 57: comparison of the time histories of displacement of the teldo at center point for different pretensions – CSD simulation

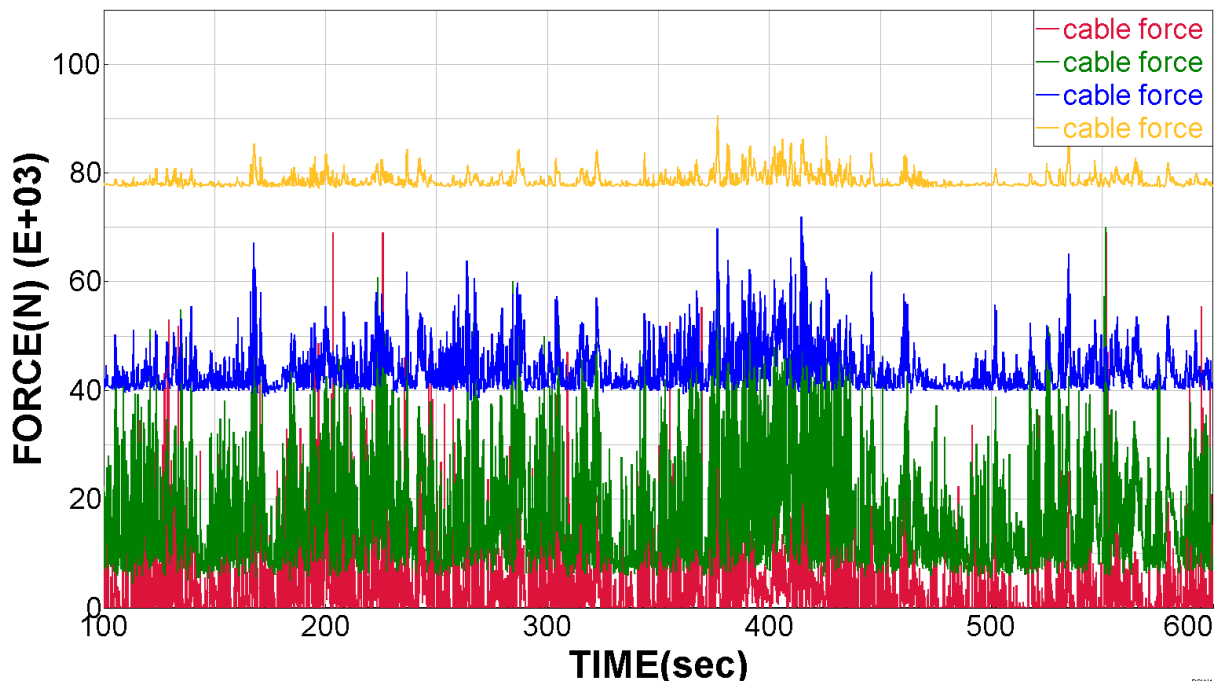
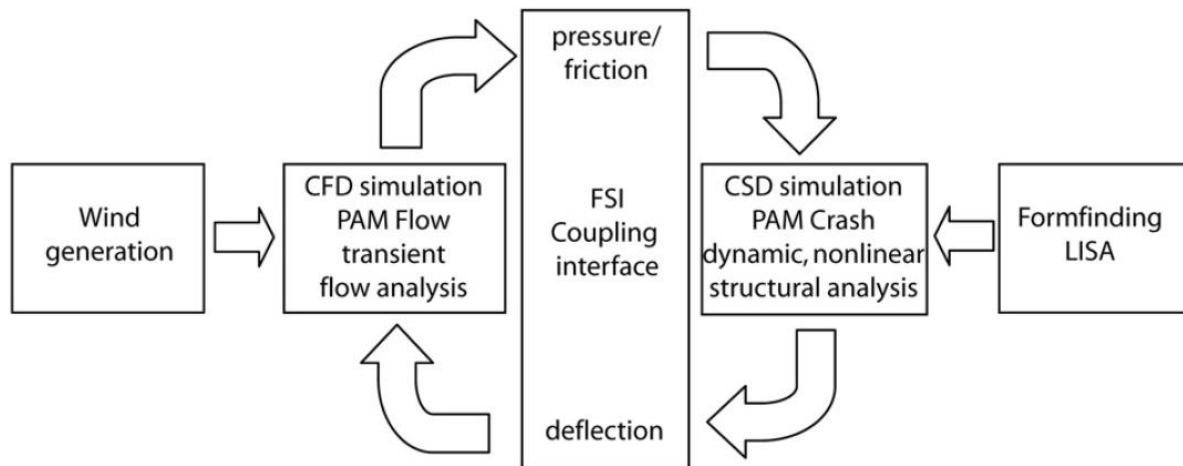


Figure 58: comparison of the middle cable force time histories for different pretensions – CSD simulation

4.3 FSI simulation

A coupled fluid-structure analysis is performed to simulate the interaction between pre-stressed cable-membrane structure mentioned in chapter 4.2.1 and wind flow which is utilized in chapter 4.2.2. The principle of the Fluid-Structure-Interaction FSI simulation is illustrated in the following chart [1].



According to this flowchart, each time step is computed at the same time for CSD and CFD models. Then at the end of each time step, the results are exchanged between CFD and CSD. The deformation is exported from CSD to CFD to generate the new geometry and the pressure is exported from CFD to CSD to update the applied load on the membrane.

The coupling conditions apply to both sides of the thin membrane, which are provided each with refined 2D surface grids connecting to the 3D CFD mesh. These grids are used to interpolate the pressures calculated in the fluid domain onto the finite element nodes of the structural model of the thin membrane. The CSD mesh density is the same as in an uncoupled CSD model. The mesh densities used on both sides of the membrane of the CFD field are identical and determined mainly from geometrical considerations (curvature, proximity of other structural parts). The interpolations required in the coupling algorithm are based on the element shape functions; loads are assembled as forces at the CFD nodes along the coupled interface, then the forces are distributed using the shape functions at the CSD nodes of the corresponding CSD element. A similar process is used for displacements. At the fluid–structure interface a no flux boundary condition is applied. This allows along the smooth surface only tangential velocity to the surface. In addition, a law of the wall is used to include friction effects. [1]

The advantage of this simulation is its accuracy comparing to other numerical methods which captures almost all the physical phenomenons. Therefore, in this study the result of FSI simulation is considered as reference and all the result of other methods are compared and evaluated with FSI.

4.3.1 CFD mesh

The mesh sizes are 30 cm around the toldo, 1.0 m in the refined region (1), 4.5 m in the refined region (2) and the background mesh is 12.5m.

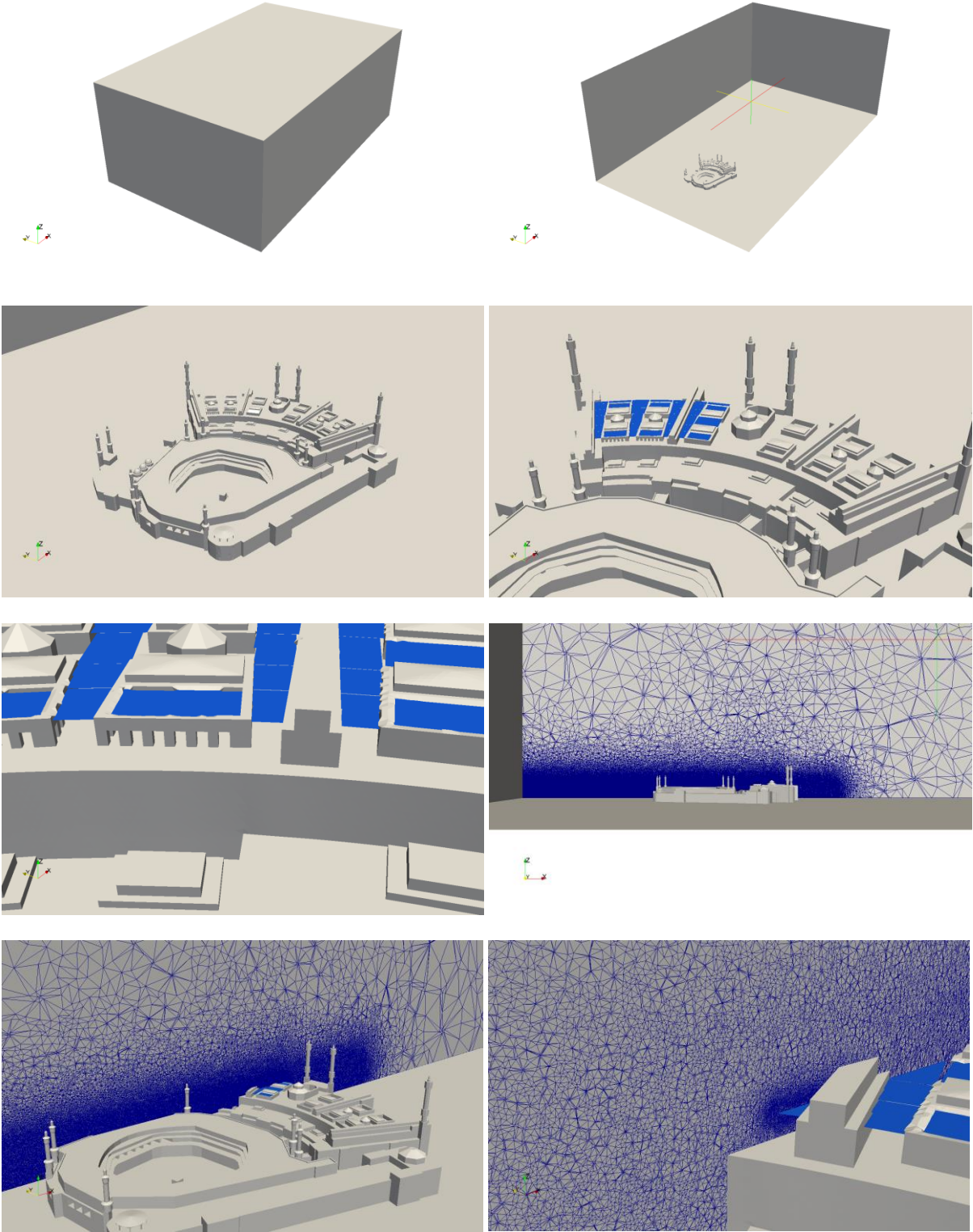


Figure 59: CFD meshed environment on the specified cut-plane and embedded toldo surfaces

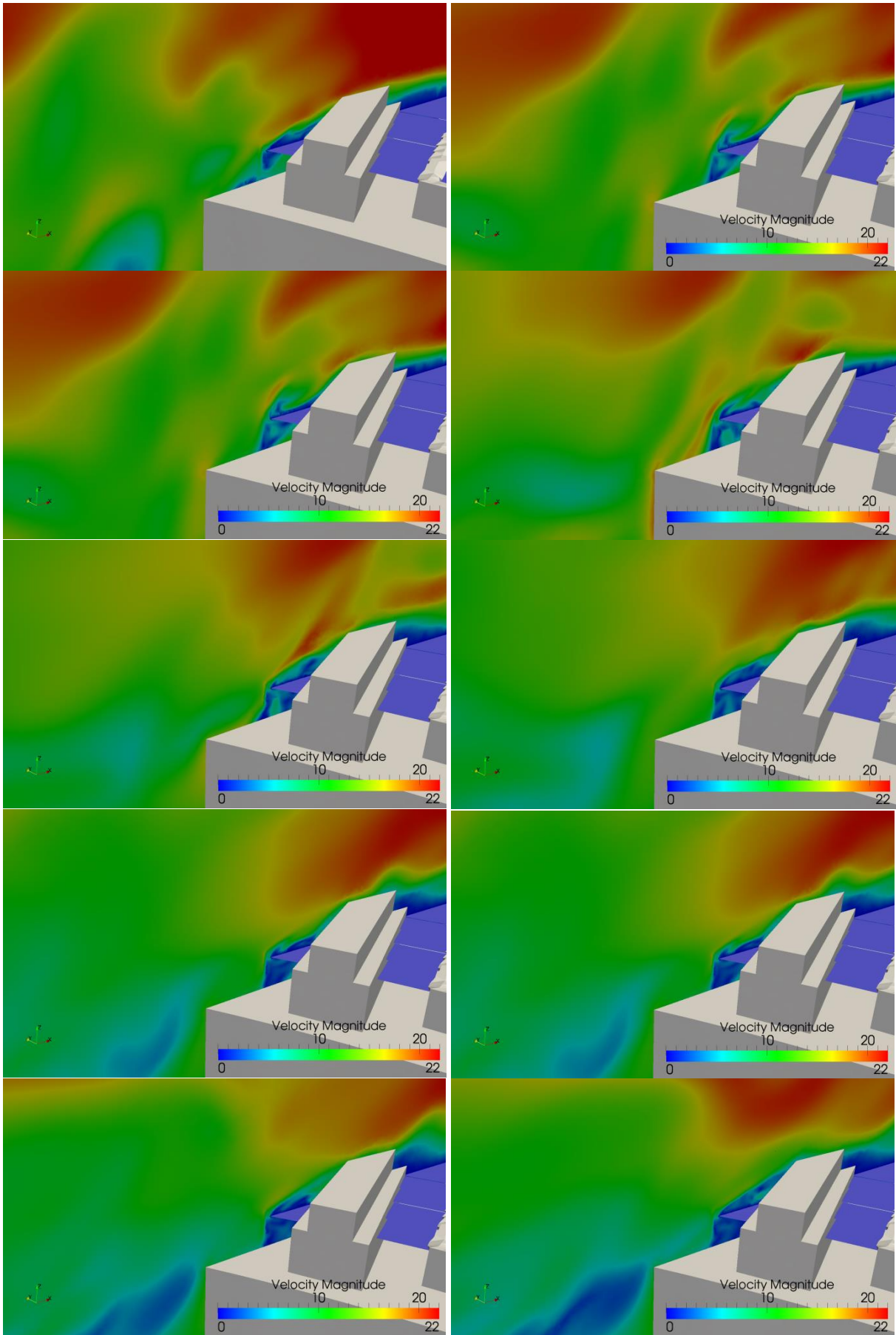


Figure 60: wind speed contour on the specified cut-plane

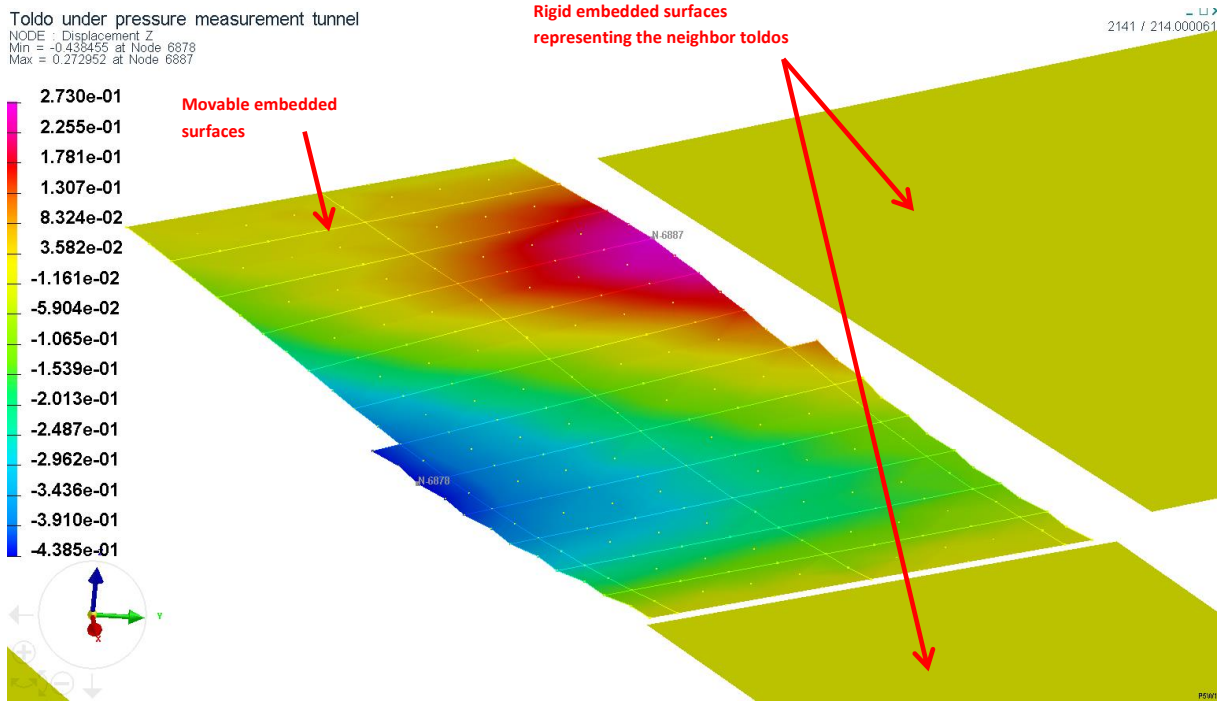


Figure 61: wind speed contour on the specified cut-plane

The results show that by increasing the cable pretension the maximum deformation of the toldo and the standard deviation of all structural responses (like deformation and cable force) are decreased. However, this is not the same case for cable force. The minimum cable reaction occurs under the 40kN cable pretension and the maximum under the 80kN. This means there is an optimum cable pretension that leads into lowest maximum cable force.

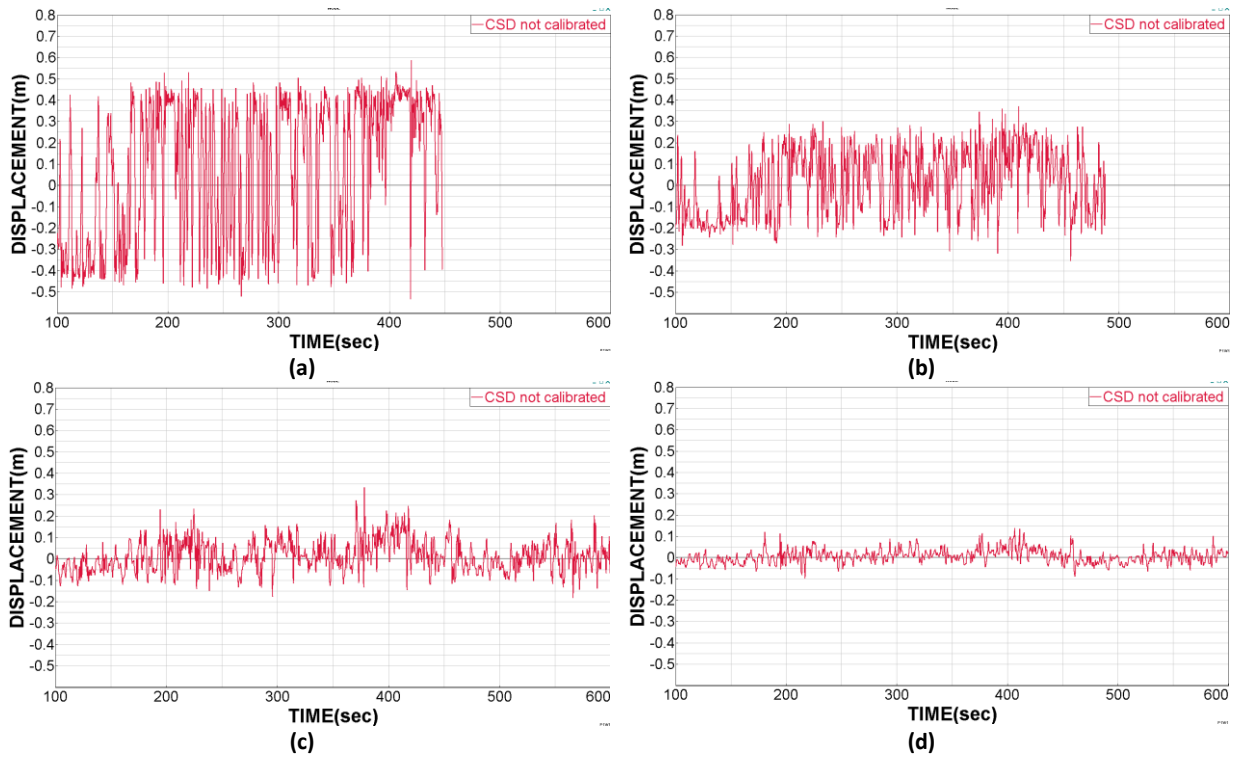


Figure 62: time history of displacement of the toledo at center point – FSI simulation (a) Pt = 10 kN, (b) Pt = 20 kN, (c) Pt = 40 kN and (d) Pt =80 kN

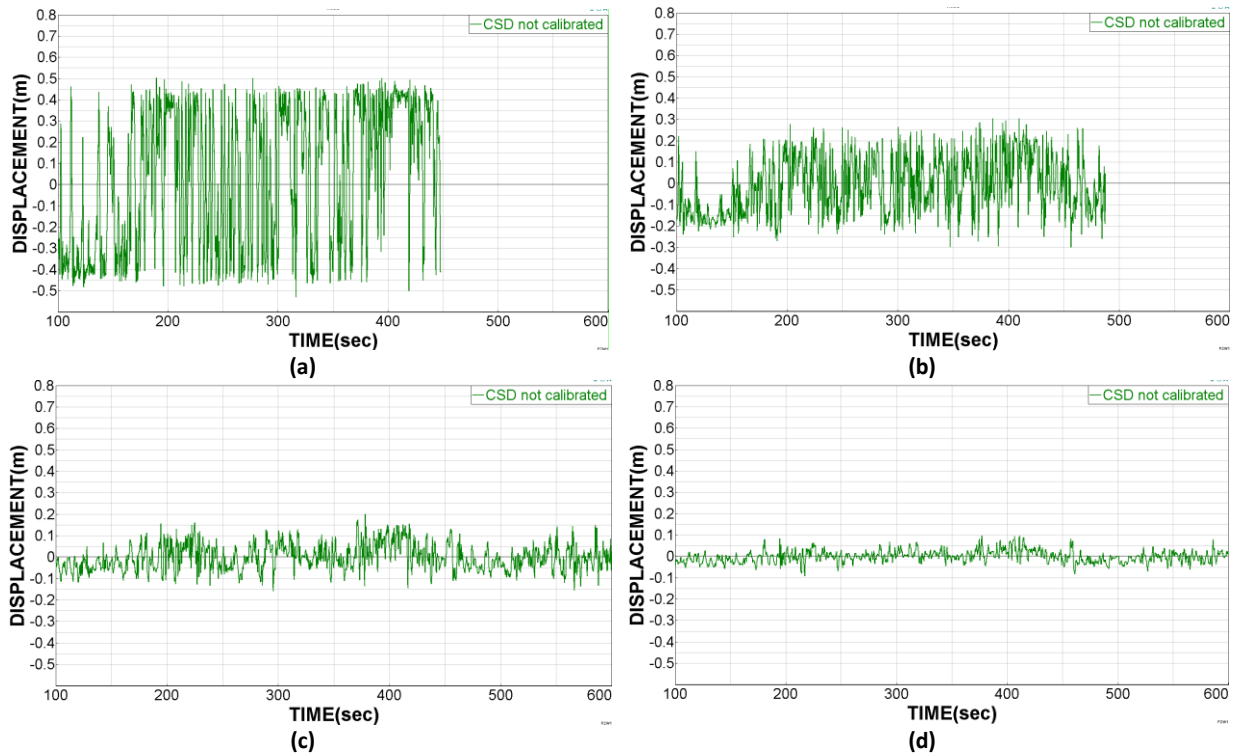


Figure 63: time history of displacement of the toledo at middle-side point – FSI simulation (a) Pt = 10 kN, (b) Pt = 20 kN, (c) Pt = 40 kN and (d) Pt =80 kN

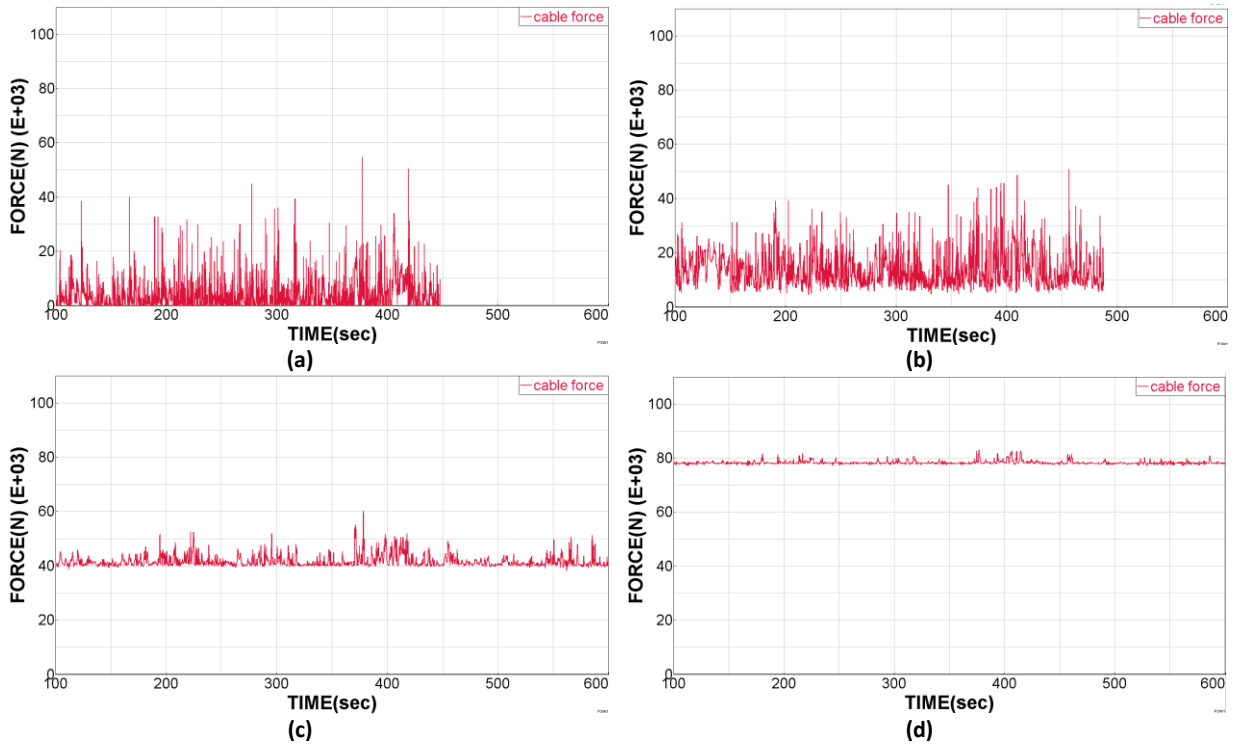


Figure 64: time history of middle cable force– FSI simulation (a) Pt = 10 kN, (b) Pt = 20 kN, (c) Pt = 40 kN and (d) Pt =80 kN

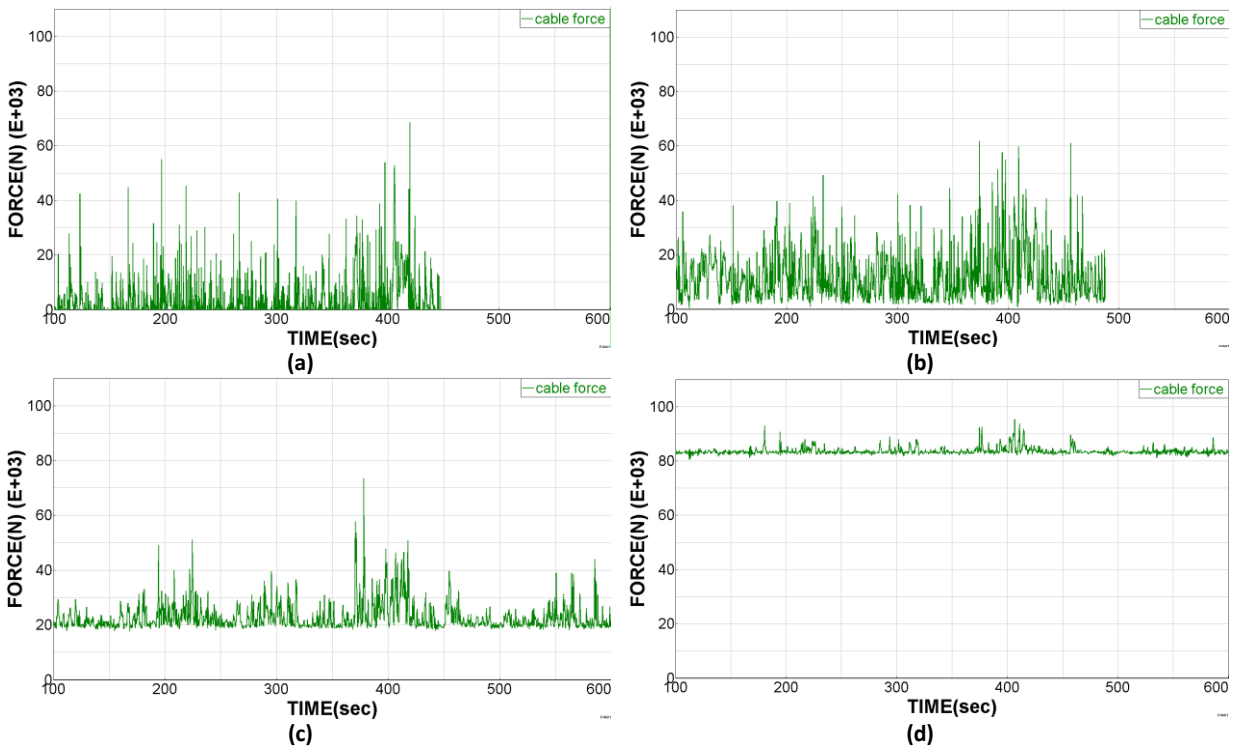


Figure 65: time history of side cable force– FSI simulation (a) Pt = 10 kN, (b) Pt = 20 kN, (c) Pt = 40 kN and (d) Pt =80 kN

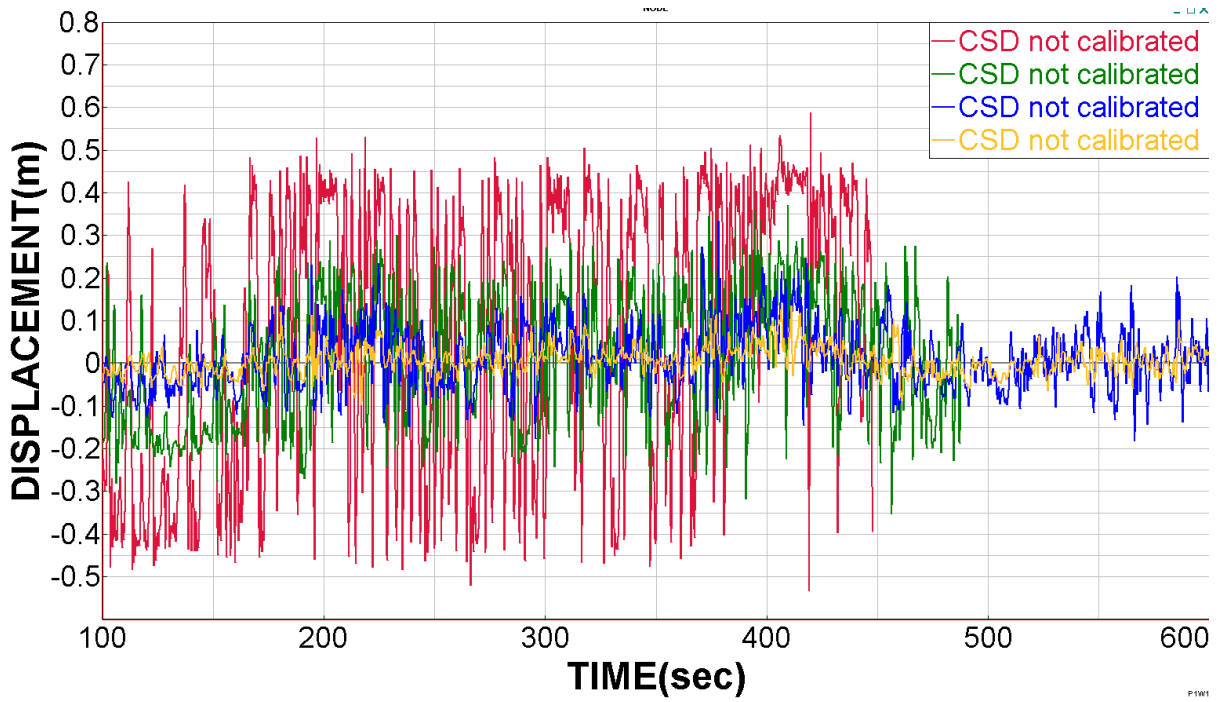


Figure 66: comparison of the time histories of displacement of the toledo at center point for different pretensions – FSI simulation

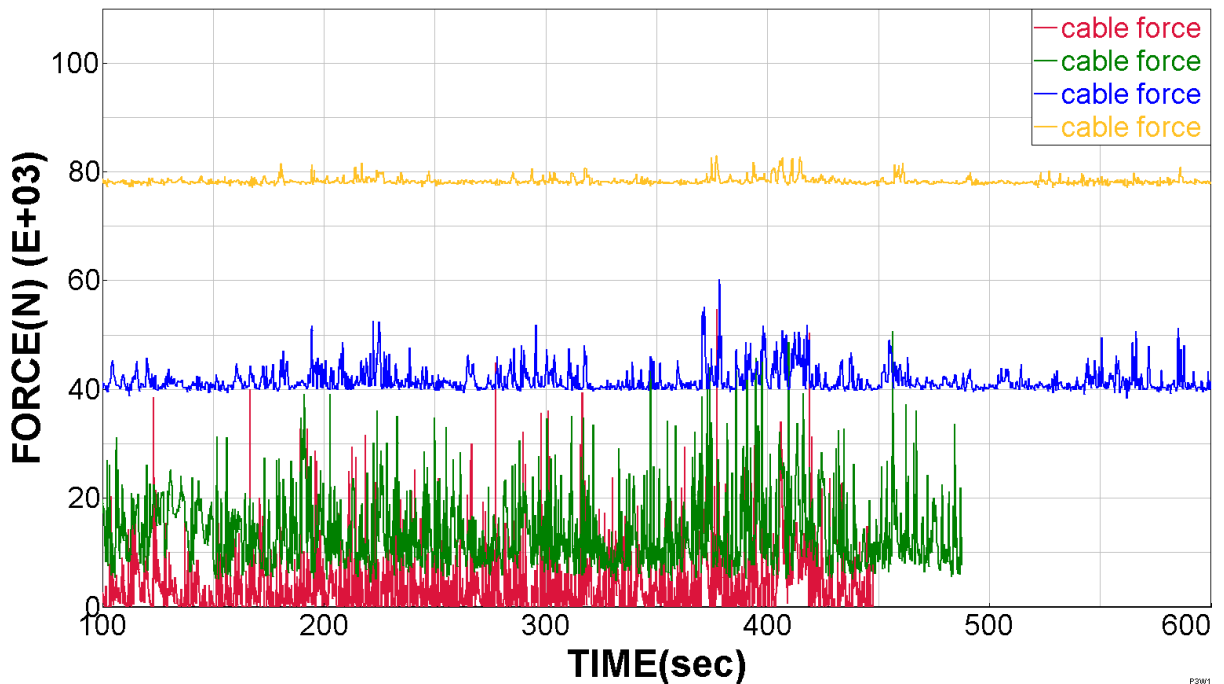


Figure 67: comparison of the middle cable force time histories for different pretensions – FSI simulation

4.4 Simulation of the calibrated CSD model

The calibrated parameters, like air added mass and aerodynamic damping, which were obtained from section 3.2 are applied in CSD model to perform dynamic time series analysis under the CFD wind pressure time series. The structural responses are presented in the following figures.

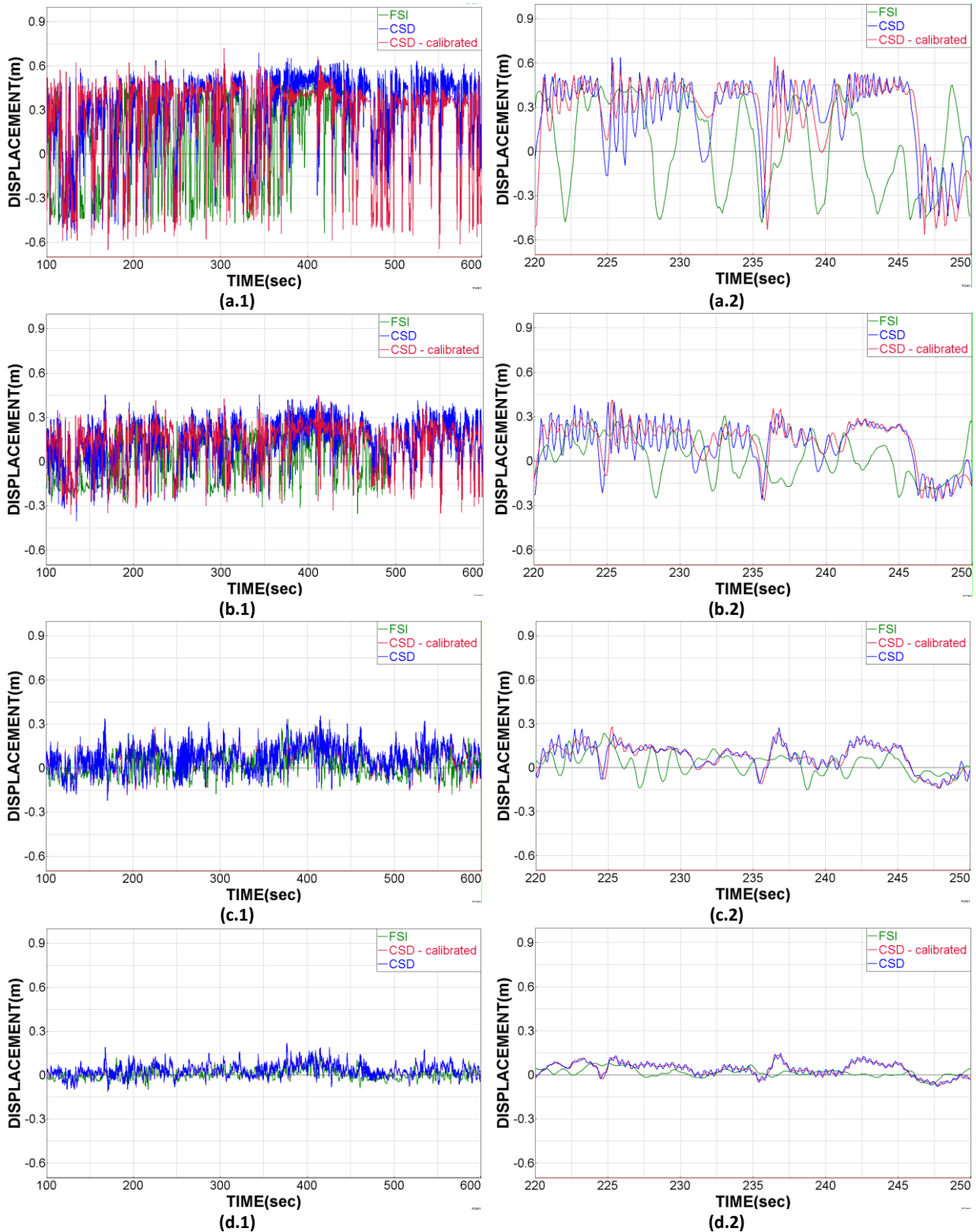


Figure 68: time history of displacement of toledo center– CSD calibrated model comparing to FSI and CSD simulations (a) Pt = 10 kN, (b) Pt = 20 kN, (c) Pt = 40 kN and (d) Pt =80 kN

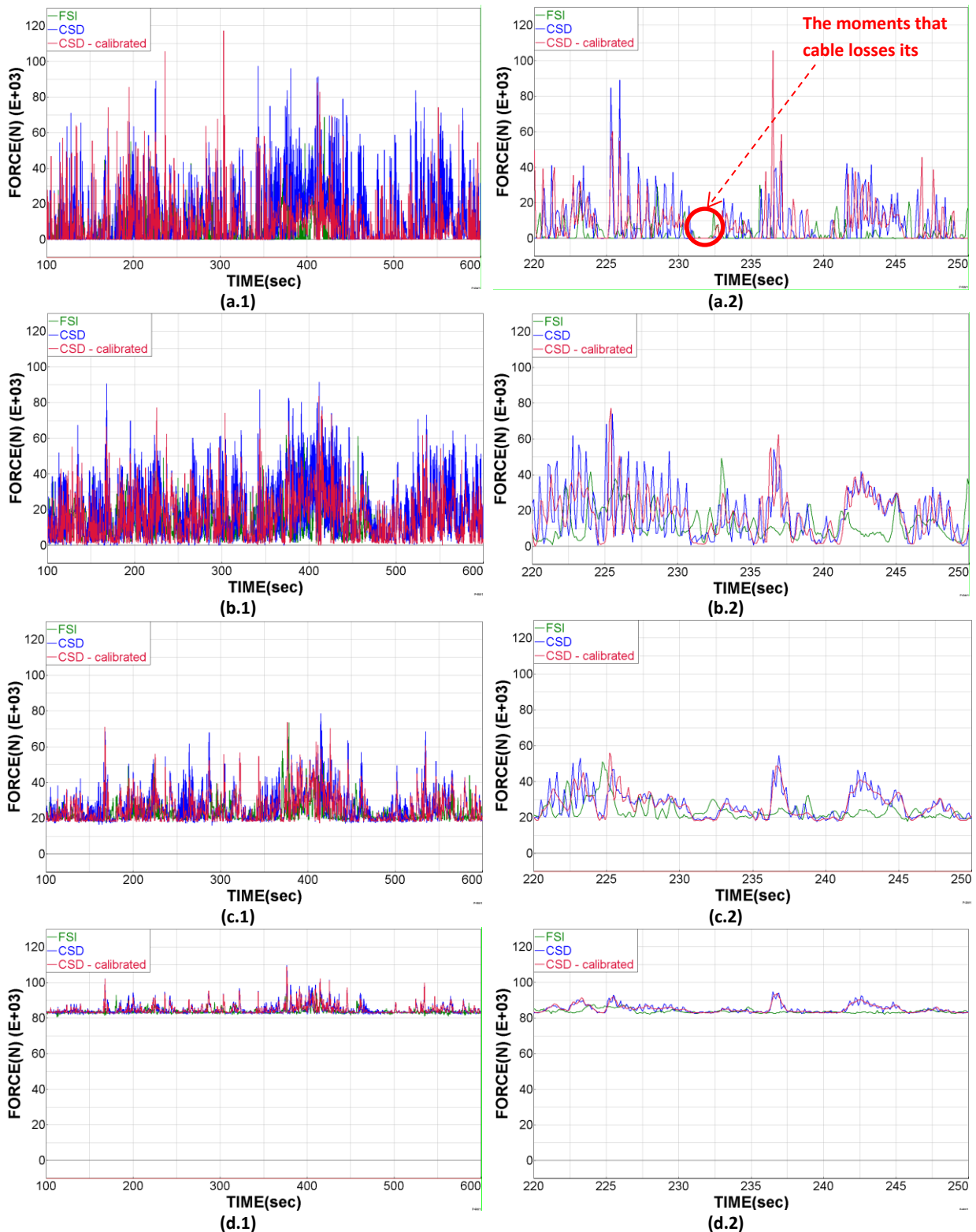


Figure 69: time history of toledo cable force middle– CSD calibrated model comparing to FSI and CSD simulations

Based on the figures above, the results of the calibrated cases mainly follow the original CSD model, but without smaller fluctuation. This is because of the higher total mass by adding the air added mass to the structure. The evaluation of the calibration would be possible by comparing the statistical form of the structural responses which is presented in 5.3.

5 Evaluation of the results and conclusion

5.1 Static analysis according to Eurocode

Reference gust wind speed of 25 m/s is considered on the eaves height of the structure ($Z = 50\text{m}$). Therefore the stagnation pressure results to $q = 0.4 \text{ kN/m}^2$.

The C_p -Value distribution is based on the DIN EN 1991-1-4:2005. Here the distributions for free standing roof according to DIN EN 1991-1-4:2005 Figure 7.6 are considered. The maximum values for inclination of the membrane between 0° and 10° are applied.

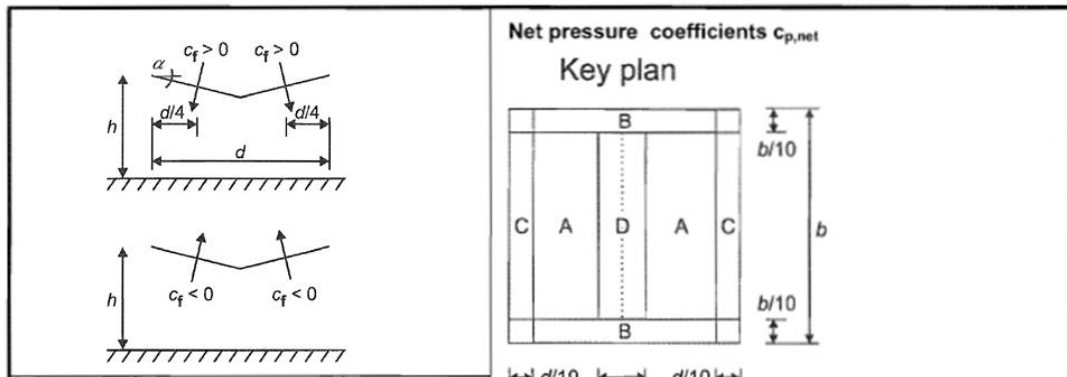
For the calculation of the umbrella structure the following c_p -values are applied:

Wind suction: $c_p = -0.7$

Wind pressure: $c_p = 0.2$

Table 2: C_p -Values according to DIN EN 1991-1-4:2005

Table 7.7 — $c_{p,net}$ and c_f values for duopitch canopies

			Net pressure coefficients $c_{p,net}$			
			Zone A	Zone B	Zone C	Zone D
Roof angle α [°]	Blockage φ	Overall Force Coefficient c_f				
-5	Maximum all φ	+0,3	+0,5	+1,5	+0,8	+0,8
	Minimum $\varphi = 0$	-0,5	-0,7	-1,3	-1,6	-0,6
	Minimum $\varphi = 1$	-1,3	-1,5	-2,4	-2,4	-0,6
+5	Maximum all φ	+0,3	+0,6	+1,8	+1,3	+0,4
	Minimum $\varphi = 0$	-0,6	-0,6	-1,4	-1,4	-1,1
	Minimum $\varphi = 1$	-1,3	-1,3	-2,0	-1,8	-1,5

The total wind loads are determined according the following formula:

$$p = q \times c_p$$

$$\text{Wind suction load case: } p = 0.4 \text{ kN/m}^2 \times -0.6 = -0.24 \text{ kN/m}^2$$

$$\text{Wind pressure load case: } p = 0.4 \text{ kN/m}^2 \times 0.3 = 0.12 \text{ kN/m}^2$$

Table 3: maximum displacement of the toldo under static wind load

Pre-tension – Pt in kN	Displacement in mm under wind suction (1 st phase)	
	Center point	Side point
10	156.4	83.3
20	181.6	110.1
40	187.5	125
80	216.7	143.5

Table 4: maximum cable force of the toldo under static wind load

Pre-tension – Pt in kN	Cable force in kN under wind suction (1 st phase)	
	Middle cable	Side cable
10	61.8	33
20	65.75	40
40	75.1	50
80	100	66

5.2 Quasi-static analysis under extreme value of the wind pressure governed from CFD-only simulation

The extreme value analysis is concerned with the determination of design values for structures subject to wind load effects. The structural design accounts for the variability and uncertainty in the wind loads by application of safety factors and by using the characteristic values of the load effects. These latter values are computed as the expected maxima given the occurrence of the 50-year wind scenario. The maxima are evaluated based on results obtained from numerical simulations of the structure for a random realization of the 50-year wind.

These results are then processed applying extreme value statistics. Two different statistical approaches are examined and demonstrated through application to exemplary simulation data sets. As shown for the investigated data sets, the limited amount of data leads to large confidence intervals of the estimates and hence to larger characteristic values. It is demonstrated that increasing the length of the simulations might – on average – reduce the confidence intervals [].

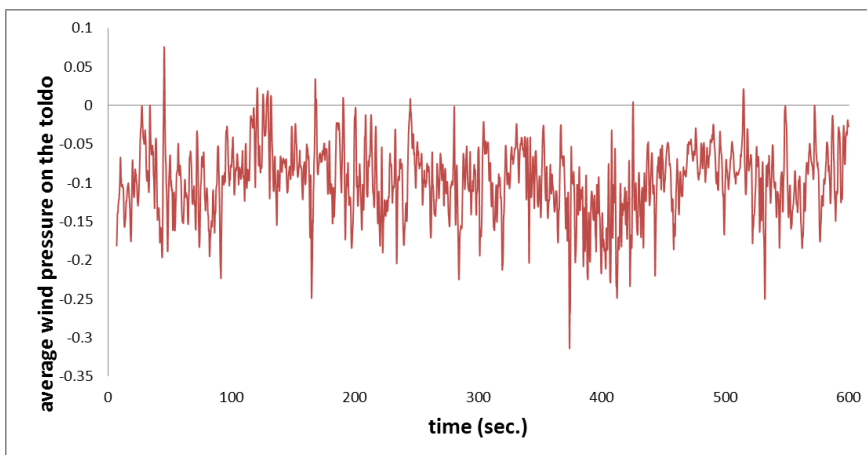


Figure 70: time history of average air pressure of the toledo from CFD wind flow simulation

The extreme value analysis is performed by a written program in Octave based on Block Maxima Modelling method. The period of interest is 600 sec. and different amount of extreme values are presented in the following table for different level of uncertainties.

Table 5: Statistic parameters of CFD wind pressure (kPa)

Maximum average wind pressure	Extreme value (Block Maxima method)
-0.31	-0.296

Table 6: quasi-static structural response of the toledo under extreme value

Pre-tension – Pt in kN	Displacement in mm under wind suction		Cable force in kN under wind suction	
	Center point	Side point	Middle cable	Side cable
10	500	470	40.5	25.8
20	353	322	60.9	39.8
40	306	219	66.6	63.6
80	212	154	88.6	88.7

5.3 Results comparison and evaluation

As it is shown in the table (8) the extreme value of middle cable force for different calculation methods are compared. The following remarks can be stated:

1. Comparing the results of case (4) with all other cases shows that cable reaction forces governed from the wind loading method of Eurocode are conservatively higher than the CFD wind simulation for different studied cable pretension in this case study. However, this could be in opposite in other case studies and depends on different parameters; therefore this evaluation cannot be stated as a global rule.
2. The Dynamic Amplification Factor (DAF) can be calculated from comparing different dynamic simulation cases (cases 0, 1 and 2) with quasi-static case (case 3). In kind of comparisons under different pretensions, by decreasing the cable pretension DAFs are increased and by increasing the pretension, DAFs tend to 1.0. In calculated DAFs for FSI simulation some factors are less than 1.0. This is because of different applied wind pressure time series in FSI simulation comparing to other cases. In FSI simulation, the toldo geometry is updated for each time-step and accordingly the wind pressure is calculated in CFD domain based on the new geometry, therefore the wind pressure time series is different in FSI. It should be noted that the applied constant wind pressure in quasi-static analysis (case 3) is computed based on the same wind pressure time series which is applied in cases 1 and 2. Therefore, DAFs for CSD in all cases are equal or bigger than 1.0.
3. The optimum cable pretension which results in the lowest dynamic amplification can be interpolated from parametric studies for any toldo case. The optimum cable pretension which is computed from this case study is around 25kN.

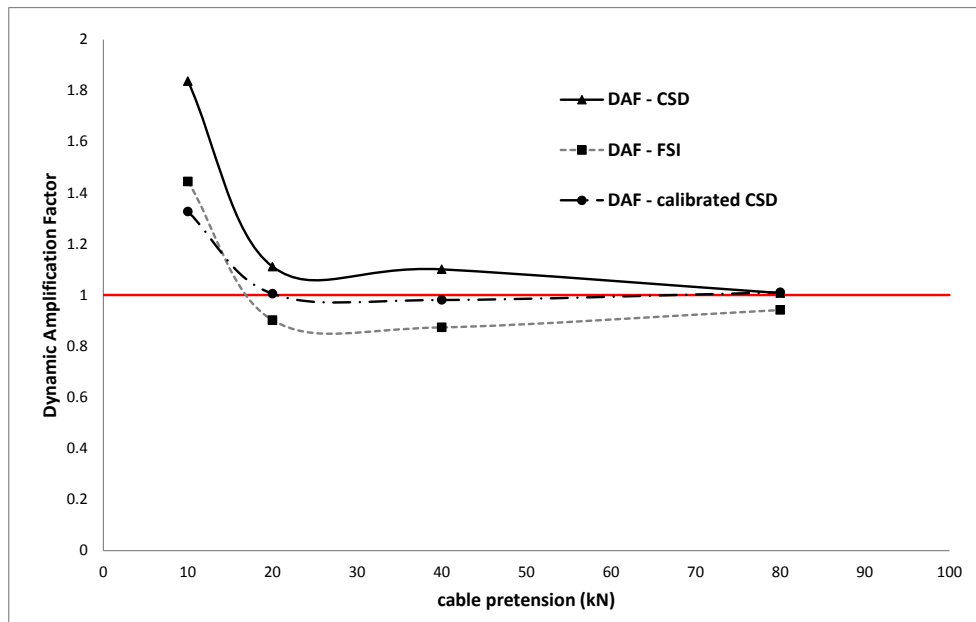


Figure 71: the variation of the dynamic amplification factor by changing the cable pretension

4. Comparing the relative difference of the standard deviations, maximums and extreme values of the cable forces for cases (1) and (2), shows for all pretensions the structural response from calibrated CSD model is closer to FSI model comparing to CSD model without calibration. The calculated error can be reduced from 27% in CSD case into maximum 12% in calibrated CSD. For more detail see table (7).

Table 7: simulation error of CSD and calibrated CSD cases comparing to FSI

Cable pretension (kN)	Error in CSD (%)	Error in calibrated CSD (%)
10	27	8
20	23	11
40	26	12
80	7	7

5. Comparing the maximums and extreme values of cable forces in all studied cases, the optimum cable pretension according to the cable reaction force is the case with 20kN pretension. However, with interpolation in the results, more precise optimum cable pretension can be extracted which is between 20kN to 30kN. This fact is illustrated in figure (74).

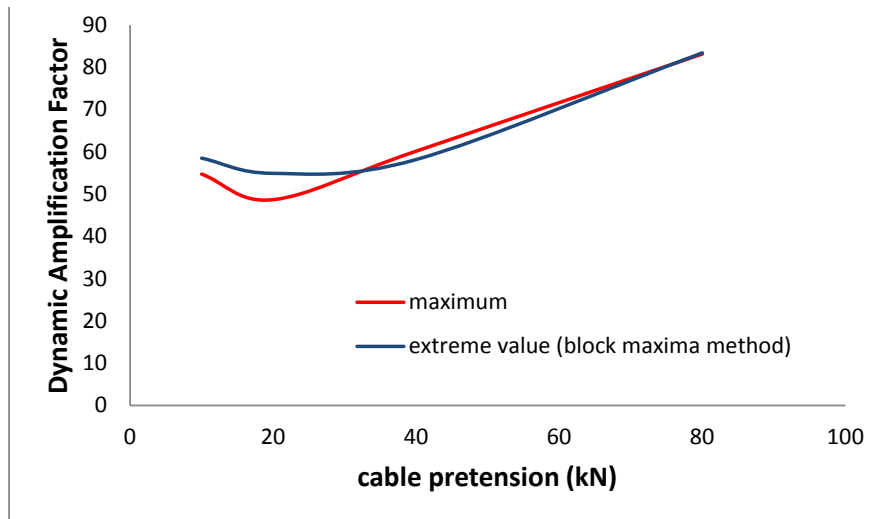


Figure 72: the variation of the dynamic amplification factor by changing the cable pretension

Table 8: Cable force in the middle cable (in kN) under wind suction

Cable pretension in kN	FSI simulation (case 0)	CSD simulation under wind pressure from CFD only simulation (case 1)	Calibrated CSD simulation under wind pressure from CFD only simulation (case 2)	Static analysis under extreme value of the wind pressure governed from CFD-only simulation (case 3)	Static analysis according to Eurocode 1991-1-4 (case 4)
10	Max: 54.7 Ext. value: 58.5 Stdv: 5.4	Max: 69.0 Ext. value: 74.4 Stdv: 7.1	Max: 52.5 Ext. value: 53.7 Stdv: 7.6	40.5	156.4
20	Max: 48.7 Ext. value: 54.9 Stdv: 6.2	Max: 60.8 Ext. value: 67.6 Stdv: 8.7	Max: 63.2 Ext. value: 61.2 Stdv: 10.3	60.9	181.6
40	Max: 60.2 Ext. value: 58.2 Stdv: 2.1	Max: 71.9 Ext. value: 73.3 Stdv: 3.8	Max: 66.0 Ext. value: 65.3 Stdv: 4.4	66.6	187.5
80	Max: 83.1 Ext. value: 83.4 Stdv: 0.66	Max: 90.5 Ext. value: 89.3 Stdv: 1.3	Max: 90.0 Ext. value: 89.5 Stdv: 1.4	88.6	216.7

References

- [1] A. Michalski, P.D. Kermel, E. Haug, R. Löhner, R. Wüchner and K.-U. Bletzinger "Validation of the computational fluid-structure interaction simulation at real-scale tests of a flexible 29 m umbrella in natural wind flow", *Journal of Wind Engineering and Industrial Aerodynamics*, 2011 P. 400-413
- [2] A. Michalski, Bernhard Gawenat, Philippe Gellenne and Eberhard Haug "Computational wind engineering of large umbrella structures", *Journal of Wind Engineering and Industrial Aerodynamics*, 2015 P. 96-107
- [3] Dieter Blümel, Rainer Graefe, Jürgen Hennicke, Friedemann Kugel, Uta Pankoke, Frei Otto, Hans-Joachim Schock and Jörg Wagner, "IL5 Wandelbare Dächer" Institut für leichte Flächentragwerke (IL) Universität Stuttgart, 1972
- [4] Hosam Alsofi, "Towards a reliable CWE simulation of dynamic wind loading on light-weight structures" Der Technischen Universität München Chair of structural analysis Prof. Dr.-Ing K.-U. Bletzinger, 2013
- [5] D. Straub and I. Papaioannou, "Procedure for Analyzing Simulation Results of Wind- induced Demands", Der Technischen Universität München, 2012
- [6] Rainald Löhner, E. Haug, A. Michalski, R. Zarfam, A. Degro, R. Nanjundaiah "Recent advances in computational wind engineering and fluid-structure interaction", *Journal of Wind Engineering and Industrial Aerodynamics*, Volume 144, September 2015, Pages 14-23
- [7] Y. Li, L. Wang, Z. Shen, Y. Tamura, "Added-mass estimation of flat membranes vibrating in still air", *Journal of Wind Engineering and Industrial Aerodynamics*, 2011 P. 815-824
- [8] B. N. Sun, J. M. Wang, W. J. Lou, "The effects of wind-induced dynamic response by added air mass for membrane structures", *Journal of Advances in Building Technology*, 2002, V2, P. 1147-1154
- [9] D. Sedlar, Z. Lozina, D. Vucina, "Experimental investigation of the added mass of the cantilever beam partially submerged in water", *Tehnički vjesnik*, 2011, P. 589-594
- [10] J. Wang, B. Sun, "Studies on Wind-induced and Vortex-induced dynamic Response of Membrane Structures", *International Journal of space structures*, 2004, V19, 167-174
- [11] S. Bingnan, S. Guohui, L. Qingxiang, "Wind-induced Dynamic analysis of membrane structures with air influence", *The fourth international symposium on computational wind engineering , CWE2006*, Yokohama, 2006
- [12] R. Wüchner, Alexander Kupzok and K. U. Bletzinger, "A framework for stabilized partitioned analysis of thin membrane-wind interaction", *International Journal for numerical methods in fluids*, 2007